

Michael Prieschl, BSc

Homogeneously Catalysed Ester Hydrogenation in Continuous Flow

A way towards a greener synthesis of Abediterol

MASTER'S THESIS

to achieve the university degree of

Master of Science

Master's degree programme: Chemistry

submitted to

Graz University of Technology

Supervisor

Univ.-Prof. Mag. Dr.rer.nat.

Christian Oliver Kappe

Institute of Chemistry

University of Graz

Graz, February 2020

AFFIDAVIT

I declare that I have authored this thesis independently, that I have not used other than the declared sources/resources, and that I have explicitly indicated all material which has been quoted either literally or by content from the sources used. The text document uploaded to TUGRAZonline is identical to the present master's thesis.

Date

Signature

Abstract

Reductions of carboxylic acid esters to the corresponding alcohols form one of the most important transformations in organic chemistry. Compared to stoichiometric reductions, the use of homogeneous catalysts and hydrogen gas for this transformation is very atom efficient and avoids the generation of hazardous waste. A homogeneously catalysed hydrogenation of a carboxylic acid ester with the commercially available catalyst Ru-MACHO is introduced into the synthetic route for the drug Abediterol. Abediterol is a newly developed drug for the treatment of respiratory disease, which is currently in phase II clinical trials. The new synthetic step replaces a stoichiometric reduction by lithium aluminium hydride (LAH).

This thesis describes the optimisation of the reaction in batch using a design of experiments (DoE) approach. It was possible to identify all side products and intermediates that are generated in the reaction. Subsequently, a homogeneously catalysed ester hydrogenation is for the first time translated to continuous flow conditions. The reaction is shown to be high yielding (98% yield, 3.7 g/h) and stable over 220 minutes of operation time using in-line ^{19}F -NMR monitoring.

It is shown that the product of the Ru-MACHO reaction can be used in the second step of the synthesis for a precursor for Abediterol. Residual Ru-catalyst does not interfere with the phase-transfer catalysed O-alkylation step. This opens up new opportunities for developing an integrated flow protocol.

Furthermore, the reaction is assessed and compared to the lithium aluminium hydride reaction concerning green metrics and factors of industrial and economical relevance. The Ru-MACHO reduction compares favourably to a typical lithium aluminium hydride reduction ($\text{PMI}(\text{Ru-MACHO}) = 14.3$, $\text{PMI}(\text{LAH}) = 51.5$). The reaction is shown to reduce the environmental impact and to be economically comparable to the currently employed route.

Zusammenfassung

Reduktionen von Karbonsäureestern zu den entsprechenden Alkoholen stellen eine der wichtigsten Umwandlungen in der organischen Chemie dar. Im Vergleich zu stöchiometrischen Reduktionen, ist die Verwendung von homogenen Katalysatoren und Wasserstoffgas sehr atomeffizient und vermeidet das Anfallen von gefährlichen Abfallstoffen. Eine homogen-katalysierte Hydrierung eines Karbonsäureesters mit dem kommerziell verfügbaren Ru-MACHO Katalysator wird in eine Syntheseroute für das Medikament Abediterol eingeführt. Abediterol ist ein neu entwickeltes Medikament, welches sich im Moment in Phase II der klinischen Studien befindet. Die neue Reaktion ersetzt eine Reduktion mit Lithiumaluminiumhydrid (LAH).

Diese Arbeit beschreibt die Optimierung dieser Reaktion im Batchreaktor mit Hilfe eines „design of experiments“ (DoE) Ansatzes. Es war möglich alle Nebenprodukte und Intermediate, die in der Reaktion auftreten, zu identifizieren. Anschließend wurde zum ersten Mal eine homogen-katalysierte Esterhydrierung unter kontinuierlichen Flow Bedingungen umgesetzt. Die Reaktion zeigt hohe Ausbeute (98% Ausbeute, 3.7 g/h) und kann stabil über 220 Minuten mit Hilfe von kontinuierlicher Analyse durch ^{19}F -NMR betrieben werden.

Es wird gezeigt, dass das Produkt der Ru-MACHO Reduktion in der zweiten Stufe der Synthese einer Vorstufe von Abediterol verwendet werden kann. Rückstände des Ru-Katalysators zeigen keinen Einfluss auf die phasentransferkatalysierte O-Alkylierung. Dies eröffnet neue Möglichkeiten zur Entwicklung einer integrierten kontinuierlichen Flow Synthese.

Weiters wird die Reaktion im Vergleich zur Lithiumaluminiumhydrid Reaktion in Bezug auf grüne Kennzahlen und Faktoren von industrieller und ökonomischer Relevanz bewertet. Die Ru-MACHO Reduktion zeigt im Vergleich zu einer typischen Lithiumaluminiumhydrid Reduktion verbesserte grüne Kennzahlen ($\text{PMI}(\text{Ru-MACHO}) = 14.3$, $\text{PMI}(\text{LAH}) = 51.5$). Es wird gezeigt, dass die Reaktion im Vergleich zur aktuellen Route die Umweltbelastung verringern kann und vergleichbare Ergebnisse in Bezug auf ökonomische Faktoren erreicht.

Acknowledgements

The present master's thesis was completed at the Institute of Chemistry, University of Graz, Austria between October 2019 and February 2020.

First of all, I want to thank Prof. C. Oliver Kappe for the opportunity to work as a part of his group on this project and for his constant support and guidance.

Next, I want to thank all my colleagues that I met while working on my thesis. Thank you for introducing me to all the equipment and for your help in the lab and office. Thank you for the warm welcome I received in the group. I want to especially thank all the PhD students I shared an office with, for all the fun we had that made completing my thesis a lot easier.

I especially want to thank Christopher Hone for directly supervising my work. Thank you for your patience and guidance during all steps of my thesis. I want to thank Jorge for his work on the topic and for introducing me to it. I also want to thank Peter for his ideas and help.

I want to thank all of my friends, the ones I made during studying in Graz and during my Erasmus stay in Ghent and the ones I have known for a long time. Especially, I want to thank my flat mates.

I also want to thank Kevin Leslie, Rachel Munday and Anne O'Kearney-McMullan from Astra Zeneca for the discussions we had and for their input during teleconferences.

Lastly, I want to thank my family. I want to thank my parents for always listening to me and for supporting me both emotionally and financially. Especially, I want to thank my brother Stefan for always listening.

This work was supported by the Research Center Pharmaceutical Engineering (RCPE) as part of the Center for Continuous Flow Synthesis and Processing (CC FLOW) project.

Table of Contents

Abstract	III
Zusammenfassung	IV
Acknowledgements	V
Abbreviations.....	VIII
1. Introduction.....	1
1.1 Ester Reductions	1
1.1.1 Stoichiometric Reductions.....	1
1.1.2 Catalytic Reductions	1
1.1.3 Homogeneously Catalysed Hydrogenation of Fluorinated Esters	4
1.2 Green Chemistry	5
1.2.1 Green Metrics.....	6
1.3 Continuous Flow Chemistry.....	8
1.3.1 Multiphasic Systems in Flow	9
1.3.2 Why Flow is Green.....	10
1.3.3 Ester Reductions in Flow	10
1.4 Statistical Design of Experiments (DoE).....	11
1.5 Abediterol	13
2. Aims of this Thesis.....	15
3. Results and Discussion	16
3.1. Optimisation in Batch	16
3.1.1 Experiments using Ru-MACHO.....	16
3.1.2 Experiments using Ru-MACHO-BH	24
3.2. Translation of the Batch Protocol to Flow.....	26
3.2.1 Identification of the Side Product.....	26
3.2.2 Optimisation in Flow	27
3.2.3 Long Run	31
3.3. Integrating the Ru-MACHO Hydrogenation into the Second Step.....	33
3.4 Comparison to the Currently Employed Route	35
3.4.1 Green Metrics.....	35
3.4.2 Industrially and Economically Relevant Factors	37
4. Conclusion and Outlook.....	39
5. Experimental.....	40
5.1 General	40
5.2 Batch Optimisation	41

5.2.1 Experiments using Ru-MACHO.....	41
5.2.2 Experiments using Ru-MACHO-BH	41
5.3 Flow Procedure for the Optimisation Experiments	42
5.3.1 Feed Preparation	42
5.3.2 Flow Procedure.....	42
5.4 Flow Procedure for the Long Run.....	44
5.4.1 Feed Preparation	44
5.4.2 Flow Procedure.....	44
5.4.3 Workup.....	46
5.5 Phase-Transfer Catalysed O-Alkylation	47
5.5.1 Feed Preparation	47
5.5.2 Flow Procedure.....	47
References	49
Appendix.....	54

Abbreviations

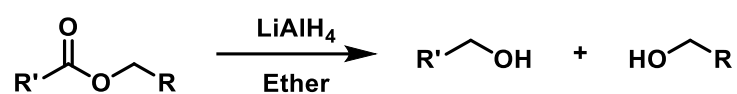
Abbreviation	Explanation	Abbreviation	Explanation
AE	Atom economy	MFC	Mass flow controller
API	Active pharmaceutical ingredient	MLR	Multiple linear regression
BPR	Back-pressure regulator	MTBE	Methyl <i>tert</i> -butyl ether
Dibal-H	Diisobutylaluminium hydride	NaOMe	Sodium methoxide
DMSO	Dimethyl sulfoxide	NMR	Nuclear magnetic resonance
DoE	Design of experiments	OE	Optimum efficiency
FD	Full factorial	PFA	Perfluoroalkoxy alkane
FFD	Fractional factorial	PMI	Process mass intensity
FID	Flame ionisation detector	PTC	Phase-transfer catalysis
GC	Gas chromatography	OVAT	One-variable-at-a-time
HPLC	High performance liquid chromatography	RME	Reaction mass efficiency
HTS	High-throughput screening	RP	Renewables percentage
IR	Infrared radiation	TBAB	Tetrabutylammonium bromide
KOMe	Potassium methoxide	THF	Tetrahydrofuran
LAH	Lithium aluminium hydride	TMS	Tetramethylsilane
LDBBA	Lithium diisobutyl- <i>tert</i> -butoxylaluminium	UV	Ultraviolet
MeOH	Methanol	WP	Waste percentage

1. Introduction

1.1 Ester Reductions

The transformation of carboxylic acid derivatives into their corresponding alcohols marks one of the most important chemical transformations in organic chemistry. The reduction of esters proves substantially more difficult in comparison to aldehydes and ketones, due to the low electrophilicity of the carbonyl carbon.^[1] Today various methods are known to perform this transformation with the desired selectivity.

1.1.1 Stoichiometric Reductions



Scheme 1.1.1: General scheme for lithium aluminium hydride ester reductions.

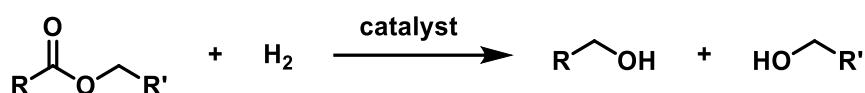
Lithium and sodium alumino- and borohydrides classically form the most important class of reducing agents used in organic chemistry for the reduction of carboxylic acid derivatives (Scheme 1.1.1).^[2] Various different derivatives of this class of compounds are available to achieve selectivity towards alcohols or aldehydes as products. While lithium aluminium hydride (LAH) is useful because of its high reducing power, it is not a very selective reagent. The less reactive sodium aluminium hydride or sodium borohydride can be used for selective reductions. To further fine tune the reactivity of the reagent LAH can be reacted with controlled amounts of alcohols or phenols to give alkoxy-aluminium hydrides. The use of diisobutylaluminium hydride (Dibal-H) is known for the selective reduction of esters to aldehydes.^[3]

The Bouveault-Blanc reaction utilising alkali metals in alcohol was widely used for the reduction of esters before the use of alumino- and borohydrides was established. Today usually improved versions of this reaction are utilised.^[4-6] The use of borane complexes has also been established for the reduction of carbonyl groups.^[7] While offering a similar reactivity as diborane (B₂H₆) they have less storage and handling concerns.

1.1.2 Catalytic Reductions

Stoichiometric reductions using alumino- and borohydrides are generally moisture sensitive and generate large amounts of hazardous waste and/or require complicated workups. Catalytic reductions, which show good atom economy and generate no waste (Scheme 1.1.2), are an ecological and economical alternative to the stoichiometric

reactions. The use of the small molecule H₂ as reducing agent is highly atom efficient and cheap, but on the other hand raises safety concerns because of its highly flammable nature. However, hydrogenations using H₂ gas are routinely performed in a safe manner at an industrial scale. Homogeneous and heterogeneous catalytic reductions of carboxylic acid derivatives have been comprehensively reviewed in 2015.^[8]



Scheme 1.1.2: General scheme for catalytic ester reductions.

Heterogeneously Catalysed Reductions

Heterogeneously catalysed hydrogenations have been described as early as 1931 by Adkins and co-workers.^[9–12] Although these Adkins-type catalysts (CuO/CuCr₂O₄) utilise very harsh conditions (>200 °C and >200 bar), these reactions utilising metal oxide catalysts are still used in modern applications for unselective reduction of fatty acids and their esters.^{[13][14]} For the reduction of unsaturated compounds, while maintaining conservation of double bonds, milder methods have been developed to facilitate the production of unsaturated fatty alcohols.^[15] More modern methods also enable the use of less harsh conditions. For example the use of a bimetallic Ag-Au catalyst has been shown to reduce dimethyl oxalate at temperatures as low as 145 °C and pressures of 30 bar.^[16]

Homogeneously Catalysed Reductions

Compared to heterogeneously catalysed ester reductions, homogeneously catalysed ester reductions can usually be operated at much lower temperatures. The first reported homogeneously catalysed ester reduction was published in 1981 when Grey and co-workers reported the use of anionic ruthenium PNN-type pincer catalysts for hydrogenation of various types of compounds.^[17–19] With this catalyst system, the scope of this reaction was still limited to activated esters with electron withdrawing groups adjacent. Piacenti and co-workers were able to show the homogeneously catalysed hydrogenation of non-activated esters, although very harsh conditions (180 °C, 130 bar) had to be applied.^[20] The group of Elsevier was able to utilise slightly less harsh conditions (100–120 °C, 70–85 bar) using a catalyst system based on Ru(acac)₃, phosphine ligands and using Zn, NEt₃ or HBF₄ as additives.^{[21][22]}

In 2006 the group of David Milstein introduced a new-type of catalyst system (**A**) utilizing pincer ligands that showed good conversions also for non-activated esters without the addition of any additives under very mild conditions.^[23] Saudan *et al* managed to overcome one of the typical limitations of active hydrogenation catalysts.^[24] They managed to demonstrate that with their catalyst system (**B**) ester reduction is preferred over olefin reduction and thus they were able to synthesise unsaturated alcohols in improved yields.

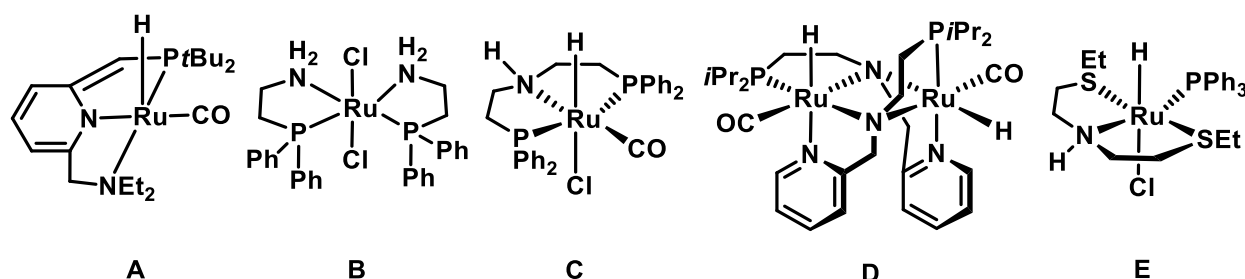


Figure 1.1.1: A selection of modern homogeneous hydrogenation catalysts.

Table 1.1.1: Comparison of the reduction of methyl benzoate with modern homogeneous catalysts.

Entry	Cat.		T [°C]	p[H ₂] [bar]	t [h]	Conv. [%]
	Catalyst	loading [S/C]				
1	A	100	115	5.3	4	97
2 ^[a]	B	2000	100	50	1	99
3 ^[a]	C	1000	100	50	16	98
4	D	20000	100	50	17	90
5 ^[a]	E	2000	40	50	3	86

^[a] Between 5-28% of NaOMe or KOMe needed for catalyst activation.

In 2011 Saito and co-workers from Takasago International Corporation introduced a ruthenium amino pincer catalyst specifically designed for industrial applications.^[25] The catalyst is called Ru-MACHO (**C**) and is available commercially. Ru-MACHO is a carbonylation resistant catalyst and is thus more effective in the reduction of methyl esters. It is able to be used in methanol as a solvent. With the catalyst it was also possible to scale up the hydrogenation of methyl (*R*)-lactate to a ton scale without significant loss of optical purity. Subsequently, the same group introduced a preactivated version of the Ru-MACHO system (Ru-MACHO-BH, Figure 1.1.2) that does not need base for activation.

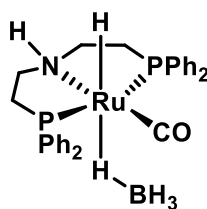
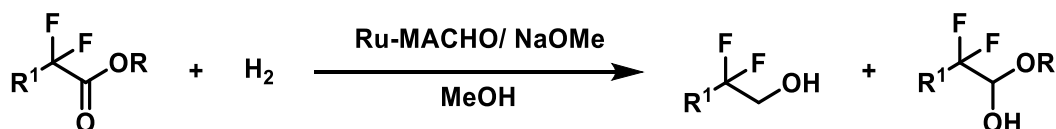


Figure 1.1.2: Structure of Ru-MACHO-BH

The group of Gusev developed very efficient Ru and Os based catalyst systems for the reduction of esters under neutral conditions.^[26] The most efficient of these catalysts **(D)** is even capable of catalysing the reduction of methyl benzoate with a substrate to catalyst ratio of 20000 (Table 1.1.1). The same group also developed a ruthenium catalyst using SNS-ligands **(E)**, which has been commercialised.^[27] This system completely avoids the use of phosphine ligands, of which the preparation can be quite costly.

Besides the homogeneous catalyst systems using Ru and Os, there are also examples known using Fe and Ir as metal centres. The group of Milstein first published catalyst systems containing a Fe centre and the group of Beller reported systems similar to Ru-MACHO containing Fe and Ir centres.^{[28][29,30]} Additionally, systems containing Mn and Co metal centres have been reported.^{[31,32][33,34]}

1.1.3 Homogeneously Catalysed Hydrogenation of Fluorinated Esters



Scheme 1.1.3: Ru-MACHO catalysed reduction of fluorinated esters.

The hydrogenation of alpha-fluorinated esters using Ru-MACHO (Scheme 1.1.3) has been investigated.^[35] It was shown that alpha-fluorinated esters are in general more reactive towards the homogeneously catalysed hydrogenations compared to beta-fluorinated and non-fluorinated esters. The hydrogenation of fluorinated esters to the alcohol product was achieved under mild conditions (40 °C, 10 atm, ester:base = 1:0.25). It was shown that by lowering temperature or base loading (15 °C, ester:base 1:0.1) it is possible to shift the selectivity of the reaction towards the hemiacetal intermediate. Increasing the hydrogen pressure was shown to decrease the amount of hemiacetal. For the substrate methyl trifluoroacetate, which forms the highly stabilised fluoral hemiacetal, it was possible to obtain the hemiacetal as main product with 89% yield on preparative scale.

1.2 Green Chemistry

In modern chemical reactions and processes not only high yield and selectivity are of importance but also the principles of green chemistry have become more important. Green chemistry in general describes the focus on chemical reactions and processes that try to avoid hazardous substances and excessive generation of waste. Green chemistry is commonly defined by the 12 principles of green chemistry, introduced by Anastas and Warner in 1998 (Figure 1.2.1).^[36] Similarly also the 12 Principles of Green Engineering by Anastas and Zimmerman and the Sandestin 9 Principles of Green Engineering have been established to assess green engineering concepts.^[37,38] In combination these principles lead the way towards more sustainable chemical processes.

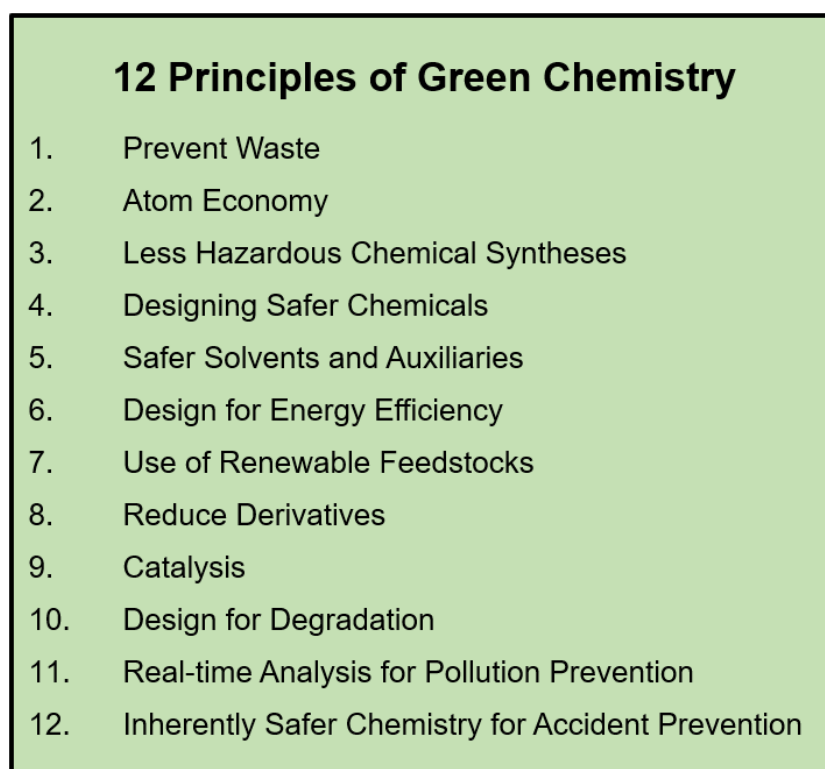
- 
- 12 Principles of Green Chemistry**
1. Prevent Waste
 2. Atom Economy
 3. Less Hazardous Chemical Syntheses
 4. Designing Safer Chemicals
 5. Safer Solvents and Auxiliaries
 6. Design for Energy Efficiency
 7. Use of Renewable Feedstocks
 8. Reduce Derivatives
 9. Catalysis
 10. Design for Degradation
 11. Real-time Analysis for Pollution Prevention
 12. Inherently Safer Chemistry for Accident Prevention

Figure 1.2.1:The 12 principles of Green Chemistry by Anastas and Warner.^[36]

1.2.1 Green Metrics

To effectively discuss how green a process is and to compare different chemical routes in terms of how green they are, a large number of different green metrics has been established. An attempt to unify reaction metrics for green chemistry has been made by John Andraos in 2005.^[39] These metrics start in a really simple manner, by using percent yield or selectivity towards the target compound and conversion of the limiting reagent as measures.

$$\% \text{ Yield} = \frac{\text{moles of product}}{\text{moles of limiting reactant}} \cdot 100$$

$$\% \text{ Conversion} = 100 - \frac{\text{final mass of limiting reactant}}{\text{initial mass of limiting reactant}} \cdot 100$$

$$\% \text{ Selectivity} = \frac{\% \text{ yield}}{\% \text{ conversion}} \cdot 100$$

Building upon those simple measures, a large variety of green metrics have been published. Some of the most important include Trost's atom economy (AE), Sheldon's environmental impact factor (E) and reaction mass efficiency (RME).^[40–42]

$$AE = \frac{\text{molecular weight of product}}{\text{total molecular weight of reactants}} \cdot 100$$

$$E = \frac{\text{mass of total waste}}{\text{mass of product}}$$

$$RME = \frac{\text{mass of isolated product}}{\text{total mass of reactants}} \cdot 100$$

Compared to bulk chemical production, manufacturing of pharmaceutical compounds generally generates much higher waste per mass of product. Process mass intensity (PMI) has been chosen by the American Chemical Society Green Chemistry Institute's Roundtable as the key parameter to assess the overall progress towards sustainable manufacturing of active pharmaceutical ingredients (APIs).^[43]

$$\text{Process mass intensity} = \frac{\text{total mass in a process or process step}}{\text{mass of product}}$$

In 2015 a unified Green Metrics Toolkit for the evaluation of the sustainability of reactions was published by McElroy *et al.*^[44] The structure of the toolkit offers four levels with increasing level of complexity on which reactions can be assessed. Starting from discovery level, through to scale-up and commercialisation all stages of chemical process development can thus be handled by the toolkit. Additionally, three new metrics have been introduced together with the toolkit. Optimum efficiency (OE), renewables percentage (RP) and waste percentage (WP).

$$OE = \frac{RME}{AE} \cdot 100$$

$$\text{Renewables percentage} = \frac{\frac{\text{mass of all renewably derivable materials used}}{\text{mass of product}}}{PMI} \cdot 100$$

$$\text{Waste percentage} = \frac{\frac{\text{total waste produced}}{\text{total mass input}}}{PMI} \cdot 100$$

In addition to the established quantitative measures, a variety of qualitative parameters are assessed by the toolkit. For laboratory scale reactions, solvents, catalyst use, energy use, the use of critical elements, batch vs flow, workup, health and safety, the use of hazardous chemicals, commercial availability and applicability of the reaction at large scale are assessed.

1.3 Continuous Flow Chemistry

The petrochemical and bulk chemicals industry is largely dominated by continuous flow processes. Historically, pharmaceutical manufacture has been performed within large-scale batch reactors. On the other hand the use of continuous flow techniques is a rather new field in research laboratories and in the manufacturing of fine chemicals such as active pharmaceutical ingredients (APIs).^[45] In the manufacturing of APIs it is crucial to be able to scale up the synthetic route very quickly if necessary. By either numbering-up of flow reactors or by scaling-up of the reactor volume, while keeping important characteristics of the system constant (“smart dimensioning”) continuous flow processes can often be transferred to larger scale with minimal adjustments. A general scheme of a simple continuous flow reactor setup for gas-liquid reaction including in-line analysis is shown in Figure 1.3.1.

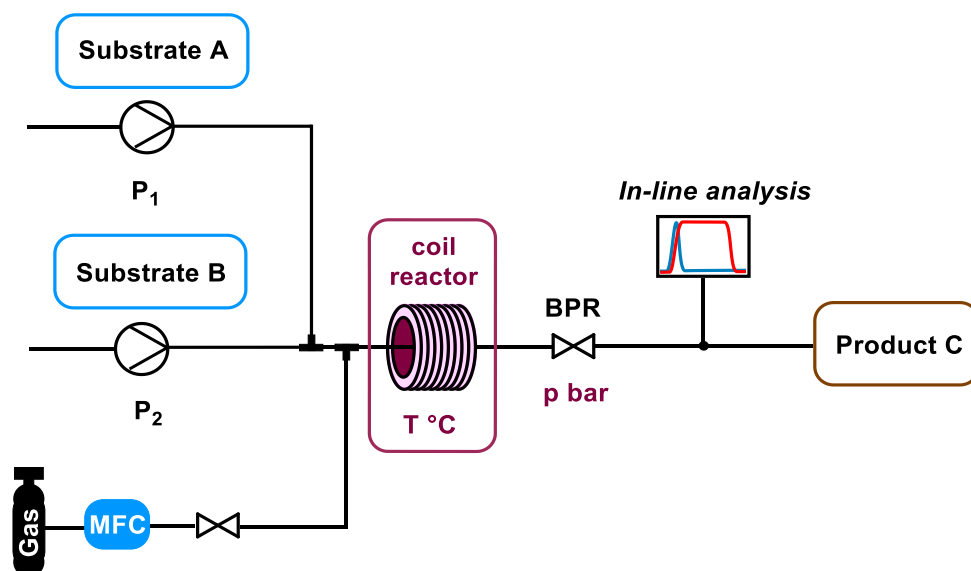


Figure 1.3.1: General scheme of a continuous flow setup for gas-liquid reactions with in-line analysis. Microfluidic flow reactors offer considerable advantages concerning mass and heat transfer, because of their high surface area to volume ratios. Thus, continuous flow offers advantages for temperature or mixing sensitive reactions. The precise temperature control also enables better selectivity towards kinetic products of reactions with small transition state energy differences. The use of flow chemistry enables the in-situ generation of chemicals that would be too dangerous to handle in a standard batch setup. The use of highly reactive, dangerous and often explosive and/or toxic chemicals (e.g., diazomethane and phosgene) can significantly shorten routes in comparison to the use of less reactive chemicals. The use of these kinds of “forbidden chemistries” in flow has been extensively reviewed.^[46]

1.3.1 Multiphasic Systems in Flow

For reactions that involve multiple phases, good interfacial mixing is crucial.^[47] For liquid-liquid reactions methods such as the use of phase-transfer catalysts that shuttle molecules from one phase to the other can be used to address the poor interfacial mixing. Through the application of microfluidic flow technology this problem can sometimes be solved by the reactor design. The decreased dimensions of the channels lead to a higher surface area to volume ratio.

For gas-liquid systems the elimination of headspace and increased surface area per reactor volume, can significantly increase the mass transfer by two orders of magnitude. Additionally, in microfluidic channels a certain type of mixing called “Taylor-Flow”, which can reduce mixing lengths significantly, can be adopted when slug flow occurs (Figure 1.3.2). Also, fluidic systems usually allow for higher pressures compared to conventional batch vessels, which increases gas solubility according to Henry’s law. One further advantage is that gaseous reagents can be precisely delivered by dosing flow volumes using mass flow controllers.^[48]

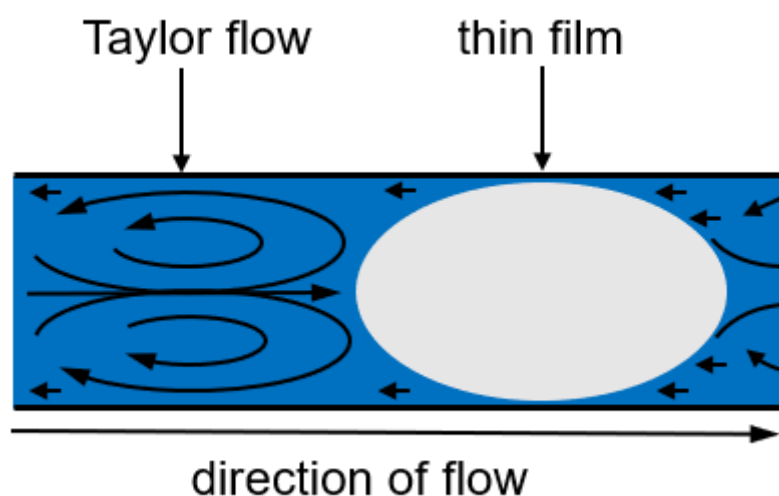


Figure 1.3.2: Taylor flow within a gas-liquid mixture in a microfluidic channel, adapted from.^[47]

1.3.2 Why Flow is Green

The influence of flow chemistry on green manufacturing has recently been reviewed.^[49] The use of continuous manufacturing is particularly interesting for developing greener processes as it contributes positively to several of the 12 Principles of Green Chemistry. Through the use of smaller reactor volumes, the severity of accidents can be reduced providing inherently safer processes.^[50]

It is often possible to increase reaction rates via high temperature, pressure and concentration.^[51] High temperature and pressure are normally not recommended by the green chemistry principles, because this intensification can be energy intensive. Although in flow these improvements can be made very efficiently, because of the small reactor volumes and high heat-exchange efficiency. This leads to more efficient processes while keeping the consumed energy low.

Real time analysis for pollution prevention is also defined as one of the twelve principles of green chemistry. Flow chemistry enables the integration of in-line and on-line analytical tools to continuously monitor reaction parameters like temperature, pressure and the progress of the reaction. Setups including in-line IR, Raman and UV/Vis spectroscopy have been reported.^[52–54] The integration of in-line NMR measurements in flow setups via benchtop NMR spectrometers has recently been established as a versatile tool for real-time monitoring of the reaction mixture.^[55] The group of Steve Ley developed an on-line miniature mass spectrometer for continuous monitoring of continuous flow processes.^[56]

1.3.3 Ester Reductions in Flow

Reductions using continuous flow systems have been reviewed by Riley *et al* in 2018.^[57] Watts and co-workers demonstrated the use of sodium borohydride in basic water solution for the reduction of an ester.^[58] The selective reduction of esters to aldehydes using Dibal-H has been translated to flow for various applications.^[59–62] Also the use of lithium diisobutyl-tert-butoxyaluminium (LDBBA) has been demonstrated to work in flow as an alternative to Dibal-H in cases where the reduction using Dibal-H was not successful.^[63] Recently the reduction of a large scope of ester substrates to their corresponding alcohols using neat borane dimethylsulfide complex was shown.^[64]

1.4 Statistical Design of Experiments (DoE)

The statistical design of experiments (DoE) is a useful and versatile statistical method that can be utilised to efficiently screen and optimise conditions for chemical reactions. DoE originates in the pioneering work of Ronald A. Fisher.^[65,66] In general, DoE can be described as a statistical tool to plan and analyse reactions to gain statistically significant insight on the optimum reaction conditions. While still being far from being a method that is routinely being used in every research laboratory, the interest in DoE has been rising in recent years.

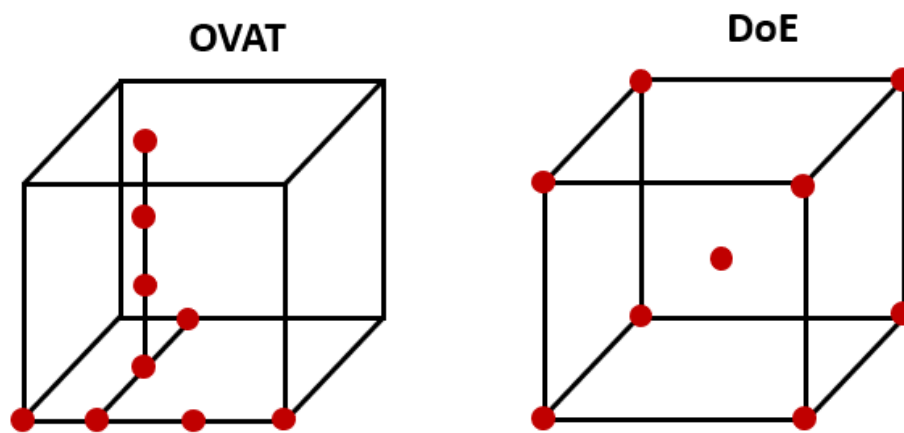


Figure 1.4.1: Distribution of experimental points: Comparison between OVAT and DoE approaches, reproduced from.^[67]

Recent publications that utilise DoE approaches for process and reaction optimisation have recently been reviewed.^{[67][68]} Compared to standard optimisation strategies that use one-variable-at-a-time (OVAT) approaches, DoE can be a far more efficient tool. By varying multiple factors at once it is possible to do more with fewer resources. Figure 1.4.1 shows a graphical representation of the distribution of experimental points in the experimental space using OVAT and DoE optimisation methods. Recent advances in high-throughput screening (HTS) tools and flow chemistry equipment enable the large set of reactions required for a DoE to be performed quickly and efficiently. By statistically assessing the results of the experiments with the automatically designed conditions, researcher bias can be eliminated. Thus, DoE is often able to uncover unexpected reaction conditions that would not be considered in a traditional OVAT optimisation. Additionally, DoE is able to detect interactions between factors.

It makes sense to use DoE either in early or in late stages of the development of a process or reaction. Early on it can be used to screen conditions at a point where not much data is available concerning the reaction. Secondly, it can be very profitable to optimise conditions for already established procedures. By minimising the use of reagents and solvents and by small improvements in yield or quality, a considerable financial impact can be made.^[69]

The different variants of DoE can be classified as screening and response surface designs.^[70] Screening designs are usually used for a first approach to a reaction to identify the factors that most influence the selected response factors. Most commonly full factorial (FD), fractional factorial (FFD) and Plackett-Burman designs are used. The full factorial, being also the most resource intensive out of the three, is the only one that enables the calculation the influence of interaction terms between the analysed factors. Response surface designs are characterised by higher experimental demand and the use of nonlinear mathematical models that enable the determination of the optimal combination of variables.

The selection of experiments that should be performed can be based on three steps^[71]: First the objectives of the project have to be defined and an appropriate strategy has to be chosen. If the reaction that is to be studied has little precedent in literature, it can be more appropriate to perform screening experiments before starting the DoE optimisation. On the other hand, if the reaction is already quite well defined it might be more appropriate to analyse the robustness of the studied reaction.

Next the experimental space has to be defined exactly by choosing the most important variables for the chosen responses (yield, selectivity, cost, etc.). Also, the ranges in which parameters are examined need to be chosen carefully. Too small ranges can lead to the optimum conditions lying outside the chosen experimental space. Too large factor ranges could generate a model that is poorly predictive. Additionally, it is important to assess which variables might actually have an impact on the final goals. Minimising the studied variables to the most important ones is a good way to minimise cost and workload.

Lastly, an appropriate design has to be chosen to determine the distribution of experiments within the experimental space. Depending on the goals and budget of the optimisation different variants of screening or response surface design can be chosen.

1.5 Abediterol

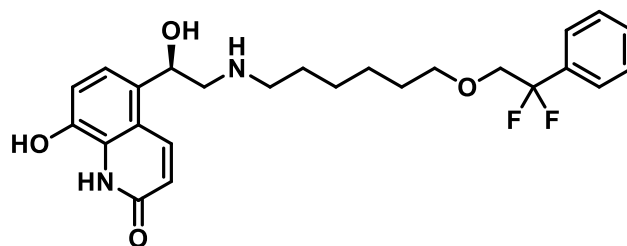
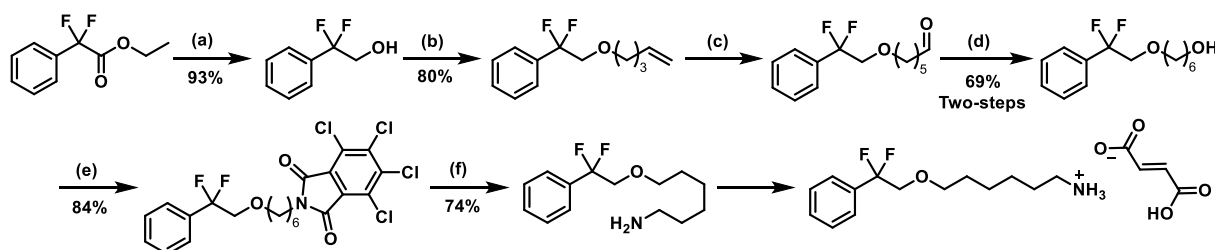


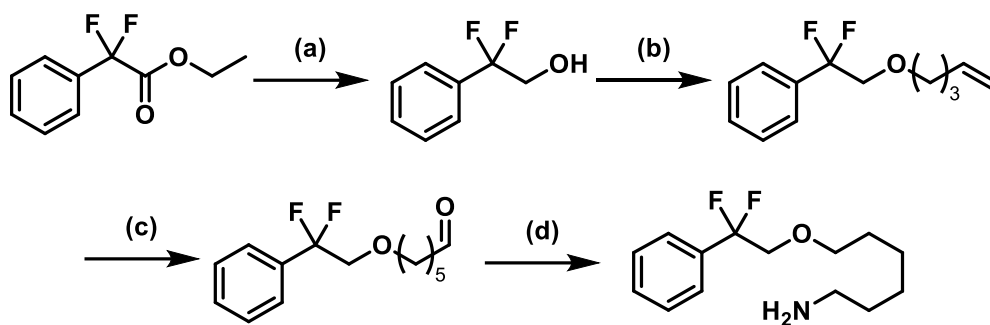
Figure 1.5.1: Structure of Abediterol.

Abediterol (Figure 1.5.1) is a potent, long-acting inhaled β_2 -adrenoceptor agonist for the treatment of asthma that was first pharmacologically characterised in 2012.^[72] A Phase I, first in-human trial showed a good safety and tolerability profile as well as a strong bronchodilatory effect.^[73] First in patient (Phase IIa) studies revealed a potent, rapid and long-acting bronchodilatory effect in asthma patients.^[74]



Scheme 1.5.1: Currently employed route for the synthesis of the lipophilic amine part of Abediterol.^[75] Reagents and conditions: (a) LiAlH_4 , THF, reflux; (b) 5-bromopent-1-ene, TBAB, NaOH (aq. 33% w/w), 70°C ; (c) $[\text{Rh}(\text{acac})(\text{CO})_2]$ (1 mol%), Xantphos (1.2 mol%), $\text{CO}:\text{H}_2$ 1:1 (3 bar), toluene, 80°C ; (d) NaBH_4 , MeOH, 0°C -rt; (e) triphenylphosphine, 3,4,5,6-tetrachlorophthalimide, DIAD, THF, 0°C -rt; (f) methylamine (aq., 40% w/w), DMF, 40°C .

The current synthetic route for the lipophilic amine part of Abediterol was published in 2019 and is shown in Scheme 1.5.1.^[75] The first step of the route is a stoichiometric ester reduction of LAH. The route employs catalytic steps such as a phase-transfer catalysed (PTC) O-alkylation and hydroformylation. But the route still includes highly wasteful stoichiometric reactions like a sodium borohydride reduction and a Gabriel type reaction that includes the derivatisation with 3,4,5,6-tetrachlorophthalimide.



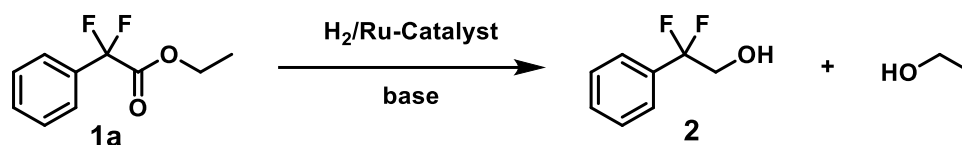
Scheme 1.5.2: Newly proposed route towards the lipophilic amine part of Abediterol. (a) Ru-catalysed ester hydrogenation; (b) phase transfer catalysed O-alkylation; (c) linear selective Rh-catalysed hydroformylation; (d) Ru-catalysed reductive amination with NH_3 and H_2 .

Previous work in our group focused on the development of a modified route for the synthesis of the lipophilic amine part of Abediterol. A route that only needs four instead of six steps (Scheme 1.5.2) was proposed. The route includes steps known from the currently employed route (step (b) and (c)), as well as newly developed steps (step (a) and (d)) and aims for the transfer of all of them to flow. Step (a) is set to use a homogeneously catalysed hydrogenation of the ester, instead of the LAH reduction that is currently employed. The new route also replaces the last three stoichiometric steps towards the amine by a catalytic reductive amination reaction. The newly developed route makes use of multiphase chemistry in all of the four steps. Three of the steps ((a), (c) and (d)) employ gas liquid biphasic systems, while step (b) employs a biphasic liquid-liquid system. All multiphase reactions are likely to benefit from the translation from batch to flow (see chapter 1.3.2).

The translation to flow allows for the safe handling of gases like H_2 and CO . Additionally, flow enables the safe intensification of these processes (see chapter 1.3.1). To our knowledge homogeneously catalysed ester hydrogenation has never been done in flow before. Phase transfer catalysed O-alkylation has been performed under continuous flow conditions.^[76,77] Advances in rhodium-catalysed hydroformylations, including continuous flow applications, have been reviewed recently.^[78] The direct synthesis of primary amines via ruthenium-catalysed reductive amination reaction (d) with ammonia and hydrogen has not yet been transferred to flow.^[79]

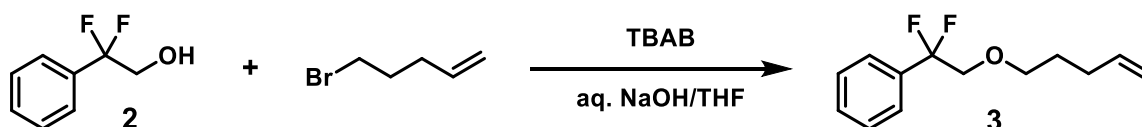
Steps (b)-(d) were already successfully optimised through previous work in our group. Optimisation and transfer to flow of step (a) are topic of the present work.

2. Aims of this Thesis



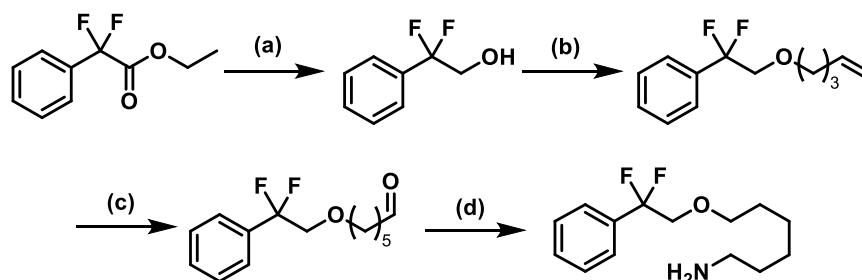
Scheme 2.1: Ru-catalysed hydrogenation of ethyl 2,2-difluoro-2-phenylacetate.

The aim of this thesis is to optimise the homogeneously catalysed reduction of ethyl 2,2-difluoro-2-phenylacetate **1a** (Scheme 2.1) to the corresponding beta-fluorinated alcohol **2** by using the commercially available Ru-MACHO as a catalyst. Another goal of the batch optimisation is to gain further understanding of the reaction in general and to understand the cause of formation of all possible side products. After the optimisation the reaction should be translated from batch to flow.



Scheme 2.2: Phase transfer catalysed O-alkylation of 2,2-difluoro-2-phenylethanol.

Furthermore, the reaction should be integrated as part of a newly modified route (Scheme 2.3) for the synthesis of the lipophilic amine part of the new drug Abediterol. The homogeneously catalysed reduction is set to replace a stoichiometric reduction of the ester by lithium aluminium hydride. For the integration of this step into the API synthesis, the goal is to show that the product generated from the Ru-MACHO catalysed ester hydrogenation can be used in the following step of the synthesis (Scheme 2.2) with minimal purification.



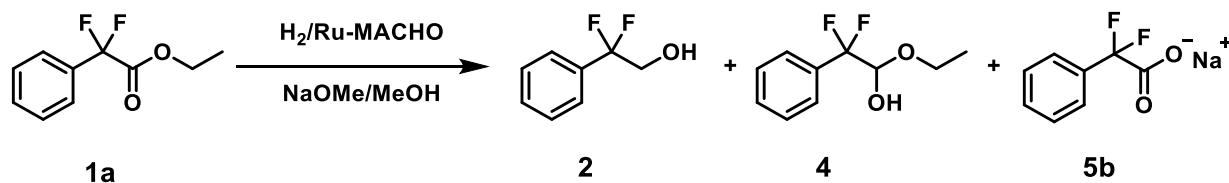
Scheme 2.3: Modified route for the synthesis of the lipophilic amine part of Abediterol.

As part of this thesis, a variety of green metrics for the newly employed ester hydrogenation shall be assessed and compared to the currently employed LAH reduction. The integration of this new catalytic step into the synthesis of Abediterol and the translation to flow should lead to a greener process in general. Additionally, some commercial factors and economic viability will be assessed.

3. Results and Discussion

3.1. Optimisation in Batch

3.1.1 Experiments using Ru-MACHO



Scheme 3.1.1: Hydrogenation of ethyl 2,2-difluoro-2-phenylacetate.

For the optimisation of the target reaction (Scheme 3.1.1) in batch a design of experiments (DoE) approach was chosen, to have a basis for further optimisation of the reaction in flow. The effect of the four parameters pressure, temperature, catalyst loading and base loading were investigated. A two-level full factorial design approach was used. Pressure was varied between 10 and 30 bar, temperature between 40 and 60 °C, catalyst loading between 0.03 and 0.1 mol% and 0.1 to 0.3 base equivalents were used. Four output parameters were chosen to be monitored: conversion of the starting material **1a**, the yield of the alcohol product **2**, yield of hemiacetal intermediate **4** and the yield of side product **5b**. The composition of the reaction mixtures after reaction was observed using ¹⁹F-NMR peak integration.

Table A1 in the appendix shows the exact parameters that were used for each of the 19 experiments that were included in the design. The design was generated using a statistical experimental design software package (Modde v11). It includes three repeats of the centre point to evaluate reproducibility (entries 17-19) and 16 conditions that are generated from a combination of the upper and lower values of the four parameters. It was observed that for experiments using 0.1 mol% of catalyst the reaction solutions were not completely homogeneous, because of the low solubility of the catalyst. This does not cause a problem in batch experiments, but for the eventual translation to flow, conditions that do not show a homogeneous solution are more challenging to handle. All batch reactions were performed in a HEL autoclave system in 25 mL stainless steel autoclave vessels.

Table 3.1.1: Results of the batch optimisation experiments.^[a]

No.	p [bar]	T [°C]	Cat [mol%]	Base [eq.]	Conv. [%]	Alcohol [%]	Intermediate [%]	Side Product [%]
1	10	40	0.03	0.1	33.0	23.3	2.3	7.3
2	30	40	0.03	0.1	72.9	66.8	1.1	5.0
3	10	60	0.03	0.1	64.7	56.9	0.5	7.3
4	30	60	0.03	0.1	>99	94.9	0.0	5.1
5	10	40	0.1	0.1	47.0	38.1	2.4	6.6
6	30	40	0.1	0.1	>99	96.3	0.0	3.7
7	10	60	0.1	0.1	99.1	93.0	0.1	5.9
8	30	60	0.1	0.1	>99	95.2	0.0	4.8
9	10	40	0.03	0.3	27.7	7.7	12.1	8.0
10	30	40	0.03	0.3	71.1	57.8	5.6	7.6
11	10	60	0.03	0.3	86.6	76.9	0.8	8.9
12	30	60	0.03	0.3	>99	94.2	0.0	5.8
13	10	40	0.1	0.3	75.1	64.3	4.7	6.0
14	30	40	0.1	0.3	>99	94.7	0.0	5.3
15	10	60	0.1	0.3	>99	94.1	0.0	5.9
16	30	60	0.1	0.3	>99	94.3	0.0	5.7
17	20	50	0.065	0.2	>99	93.8	0.0	6.2
18	20	50	0.065	0.2	>99	94.7	0.0	5.3
19	20	50	0.065	0.2	>99	95.2	0.0	4.8

^[a]Standard reaction conditions: 5 mmol of **1a**, 2.5 mL of MeOH, stirring at 600 rpm for 1 h. Conversion and product distribution determined by ¹⁹F-NMR.

Table 3.1.1 shows the results from the batch experiments of the DoE. Very high conversion was achieved for a variety of conditions. The chosen centre point conditions (entries 17-19) resulted in full conversion and high selectivity towards the alcohol product **2**. In general, only small amounts of the hemiacetal intermediate **4** were found. No statistical model could be fitted to the data generated for the amount of **4** formed in the reaction. The highest amount of intermediate (12.1%) was formed using low temperature, pressure and catalyst loading with high base loading (Table 3.1.1, entry 9).

For the conversion of the starting material no statistical model was fitted, because full conversion was reached for 10 out of 19 experiments. Thus, no significant difference between the conditions could be observed using this parameter.

Statistical models were generated for the amount of product **2** and the amount of side product **5b**. Models were generated using multiple linear regression (MLR) by including all main and interaction terms and then non-significant terms were removed. A good fit for both models was reached.

The fit for the percentage of formed product **2** (Figure 3.1.1) showed an R^2 value of 0.79 and a Q^2 value of 0.65, which suggests a good level of predictability. The model validity shows a negative value, which is caused by the very high reproducibility. Confidence in the model is given by the acceptably high Q^2 value. Pressure, temperature and catalyst loading were shown to have a positive influence on the formation of the alcohol product. The base loading did not show an influence on the amount of product that was formed.

One interaction term (pressure*temperature) was shown to have a negative influence on the amount of product that was formed. This shows that some kind of non-linear interaction is influencing the amount of product that is formed. It was shown that the inclusion of an arbitrary squared term (temperature squared) improves the fit up to a R^2 value of 0.89 and a Q^2 of 0.77 (Figure 3.1.2). This shows that curvature definitely plays a role for at least one parameter. With the amount of experiments that were performed it was not possible to identify which of the parameters shows curvature. To accurately identify non-linear influences of the variables it would be necessary to adopt a response surface design, which uses nonlinear mathematical models. For example, using a central composite design, it would be possible to show the influence of which parameter actually shows curvature. For this, further experiments would be needed to be performed. As the reaction was set to be translated to flow, no further investigations in batch were conducted.

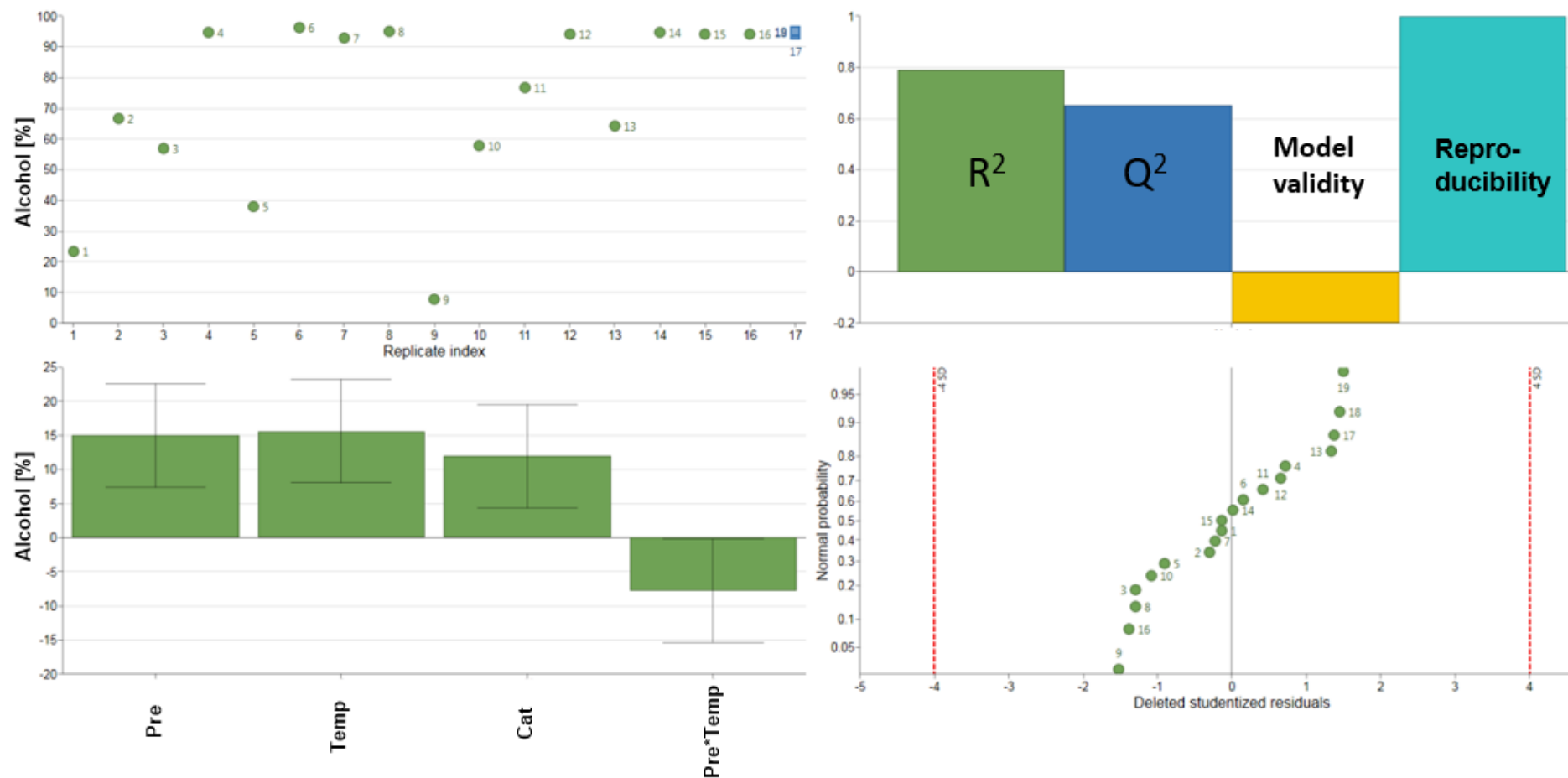


Figure 3.1.1: Summary of the fit for the linear model generated for the amount of formed product **2**. The top left shows the replicate index versus the amount of alcohol product that was formed. In the top right a summary of the most important parameters regarding the fit is shown (R^2 , Q^2 , model validity and reproducibility). The bottom left shows all parameters that were found to have an influence on the product formation. The bottom right shows the statistical distribution of the residuals of the measured values.

The top left graph in Figure 3.1.1 shows the replicate indices and the spread of data over all experiments. The data points for the different conditions show values between 7.7% (entry 9) and 96.3% product (entry 6). The blue rectangles represent the repeats that were done for the centre conditions. The data for the repeats only spreads from 93.8% to 95.2% product. This shows that the reaction is highly reproducible. The bottom right graph shows the statistical distribution of the residuals of the measured values. The residuals show a normal distribution without any outliers. Graphs, which compare the observed values against values predicted by both the linear and square model for all measured conditions, are shown in the appendix (Figure A4 and A5).

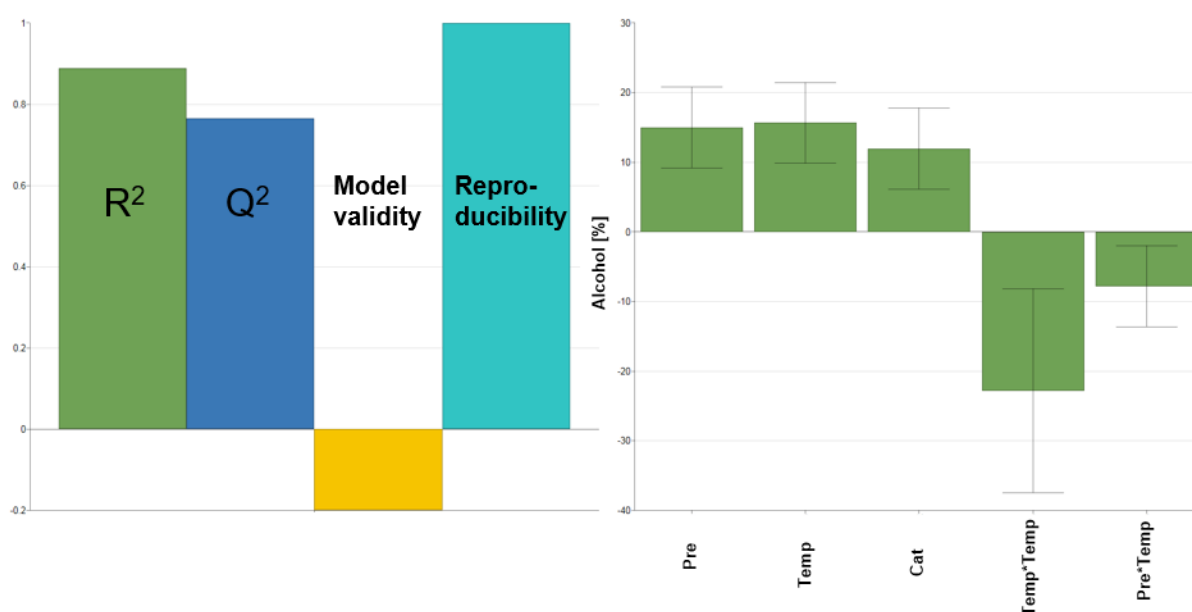


Figure 3.1.2: Summary of the fit for the model including curvature for the amount of formed product 2. The left graph shows the most important parameters regarding the fit shown (R², Q², model validity and reproducibility). The right graph shows all parameters that were found to have an influence on the product formation. The term Temp*Temp is chosen arbitrarily to show the influence of curvature.

The generated models can be used to determine optimum conditions for further reactions. The influence of the different parameters on the amount of formed product is shown graphically in the form of contour plots. The influence of temperature and pressure for the linear model is represented in Figure 3.1.3. A general summary of the influence of pressure, temperature and catalyst loading is shown graphically in Figure A3 in the appendix.

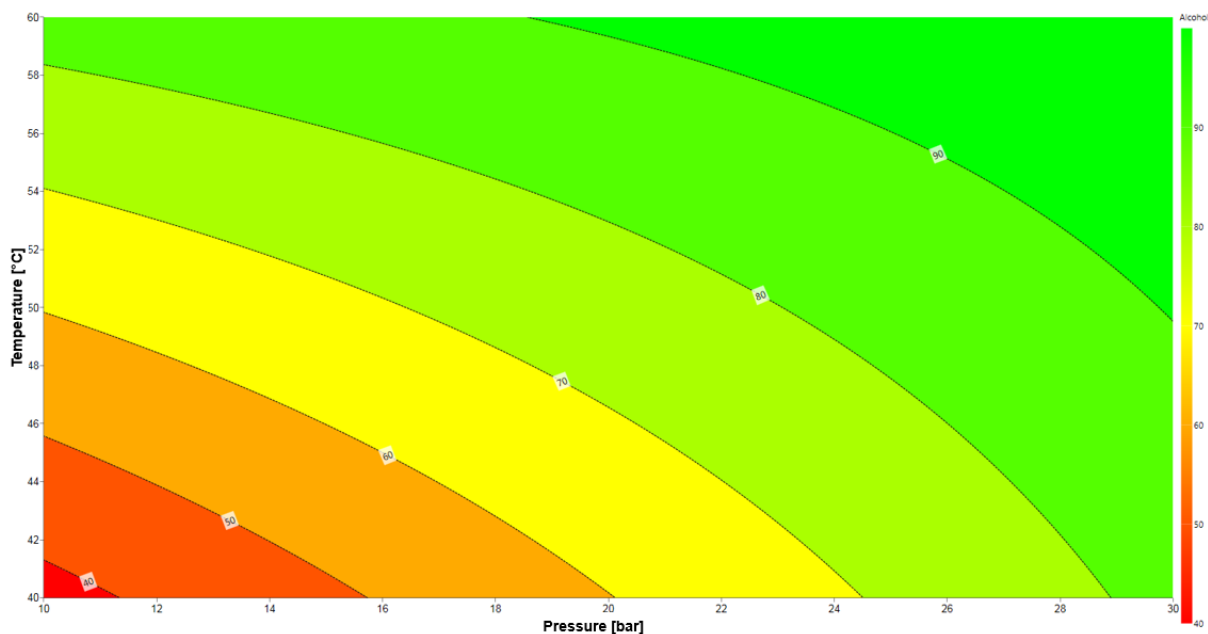


Figure 3.1.3: Contour plot showing the influence of temperature and pressure on the formation of alcohol product **2**.

The fit for the amount of side product **5b** that is formed (Figure 3.1.4) shows an R^2 value of 0.72 and a Q^2 of 0.57. The model also shows high model validity and high reproducibility. Three parameters were shown to have an effect on the amount of **5b** formed during the course of the reaction. Increasing the pressure and the catalyst loading decreases the amount of **5b** that is formed, while increasing the base loading increases the amount of **5b**. The top left graph shows the spread of data and the replicate indices. The data from the experiments with different conditions spread between 3.7% and 8.9% of side product. The blue square data points representing the repeats show a much smaller spread between 4.8% and 6.2% side product, thus showing high reproducibility. Compared to the fit for product **2**, the relative spread is much higher, but the absolute spread of the replicates is similar. The bottom right graph, which shows the statistical distribution of the residuals of the measured values, shows a normal distribution without any outliers. A graph comparing the measured values against the values predicted by the model is shown in the appendix (Figure A6).

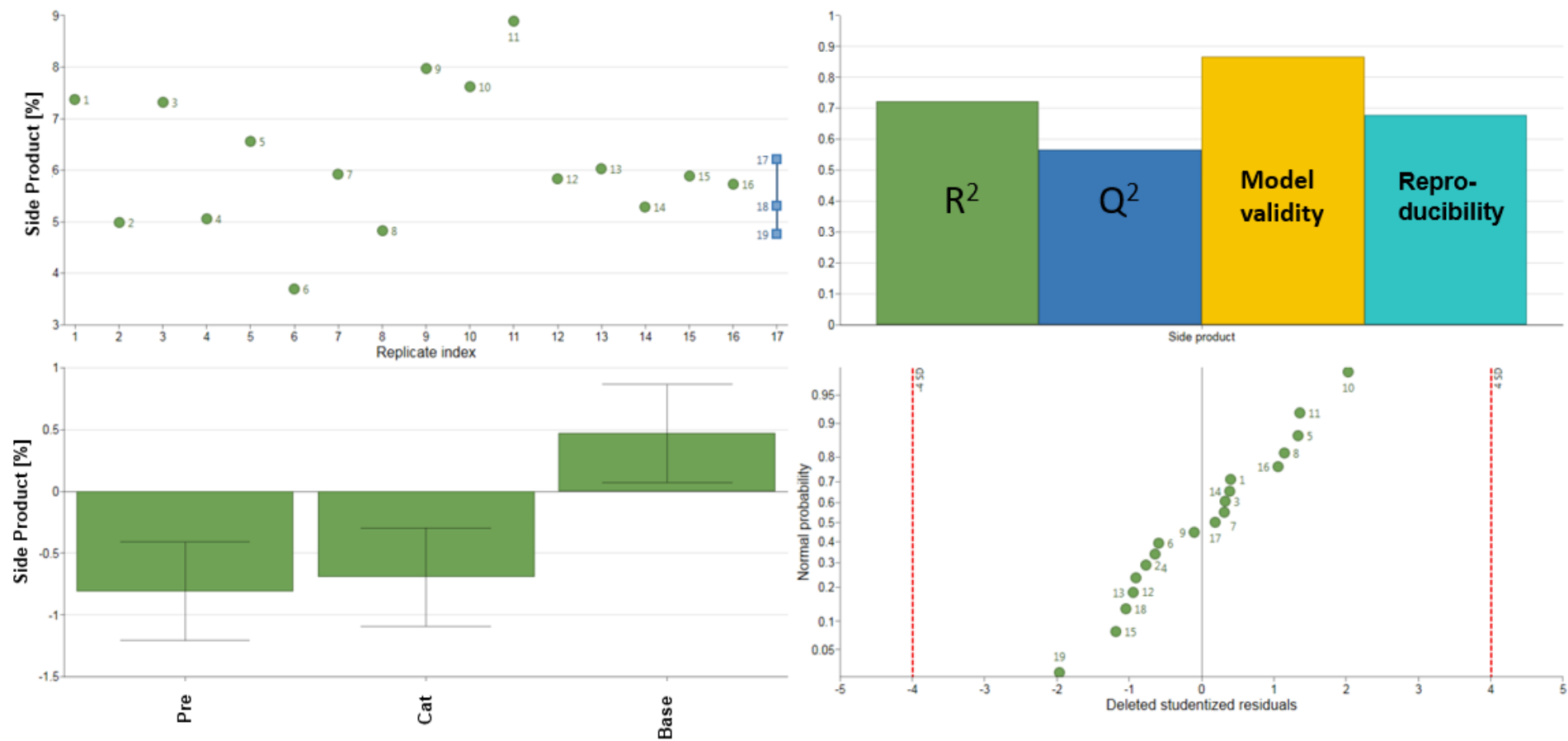


Figure 3.1.4: Summary of the fit for the linear model generated for the amount of formed side product **5b**. The top left shows the replicate index versus the amount of side product that was formed. In the top right a summary of the most important parameters regarding the fit is shown (R^2 , Q^2 , model validity and reproducibility). The bottom left shows all parameters that were found to have an influence on the side product formation. The bottom right shows the statistical distribution of the residuals of the measured values.

3.1.2 Experiments using Ru-MACHO-BH

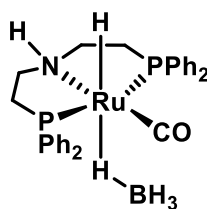


Figure 3.1.5: Structure of Ru-MACHO-BH

The experiments of the DoE showed that the amount of base in the reaction increased the formation of side product **5b**. The preactivated catalyst Ru-MACHO-BH (Figure 3.1.5) that has been reported for working without base was tried out to avoid the formation of the side product completely. To ensure good comparability to the experiments from the DoE, initial experiments were conducted using similar conditions to the centre conditions of the DoE with the preactivated catalyst and no addition of base.

Table 3.1.2: Results from the experiments using Ru-MACHO-BH as a catalyst.^[a]

Entry	Temperature [°C]	Pressure [bar]	Cat. Loading [mol%]	Base [eq.]	Conc. [mol/L]	Conversion [%]	Alcohol [%]
1	50	20	0.076	0	2	0	0
2	50	20	0.076	0.2	2	>99	98

^[a]Standard reaction conditions: 5 mmol of **1a**, 2.5 mL of MeOH, stirring at 600 rpm for 1 h. Conversion and product formation determined by ¹⁹F-NMR.

Table 3.1.2 shows the results from the experiments using Ru-MACHO-BH as a catalyst. Without the addition of base, the catalyst showed no activity and no substrate was converted to product. For control reasons the same reaction was also done with the addition of 0.2 equivalents of sodium methoxide (NaOMe) (entry 2). The catalyst showed excellent reactivity and selectivity when 0.2 equivalents of base were added.

This leads to the assumption that the catalyst was deactivated by the short exposure to air, during sample preparation. The borane group that is attached to the ruthenium atom in the Ru-MACHO-BH catalyst is probable to be hydrolysed by the exposure to air moisture, which leads to deactivation of the catalyst. This assumption was proven by taking ¹H-NMR spectra of the catalyst under inert conditions and after exposure to air. Figure 3.1.2 shows an overlay of ¹H-NMR spectra before and after exposure to air. The signals corresponding to the protons attached to the boron are easily assigned in the spectrum taken under inert conditions (bottom spectrum) between -0.73 ppm and

0.08 ppm because of the distinct coupling pattern of the protons to ^{10}B and ^{11}B . In the second spectrum taken after exposure to air (top spectrum), these peaks are no longer found. It is also clearly visible that the peak at 3.33 ppm corresponding to water is much larger after exposure to air. From this evidence it is clear that the catalyst is deactivated quickly, if it is not handled under glovebox conditions. Because the operation of all steps under glovebox conditions was not viable, no further experiments were conducted using the Ru-MACHO-BH catalyst.

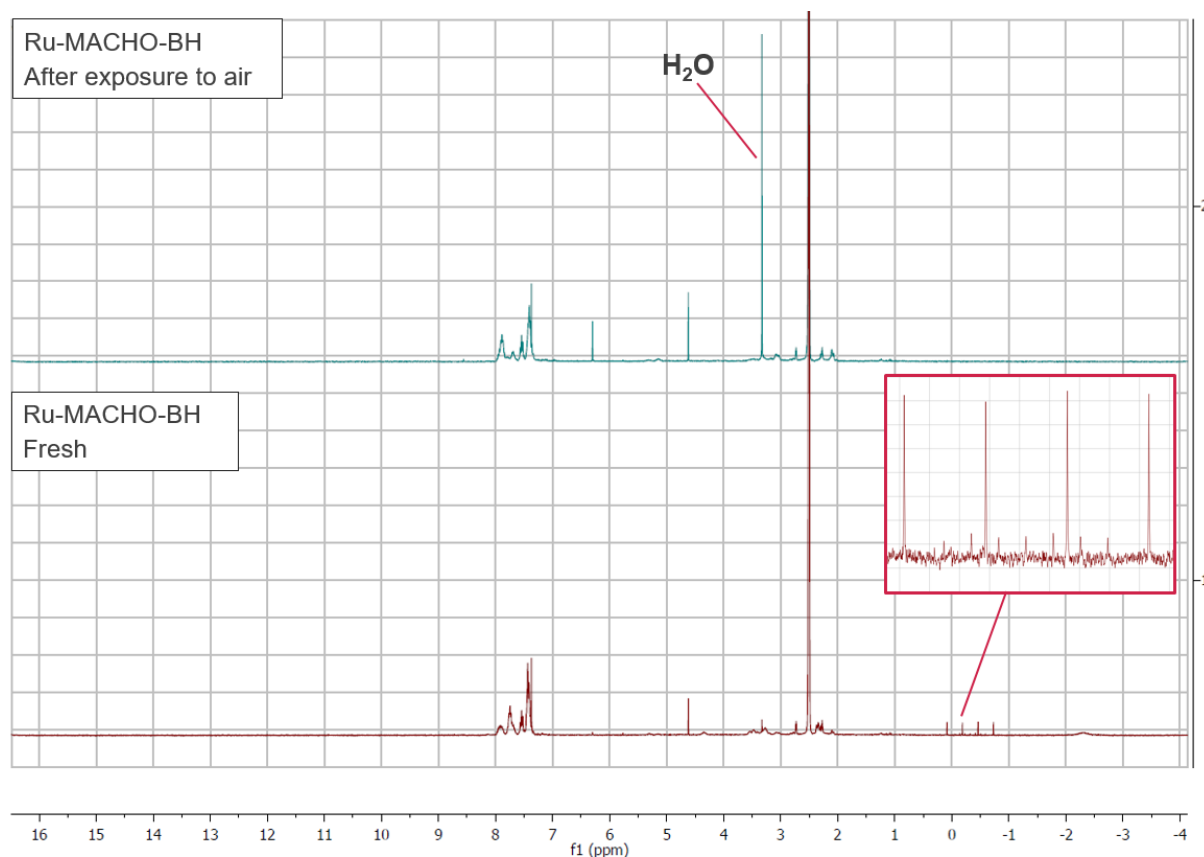


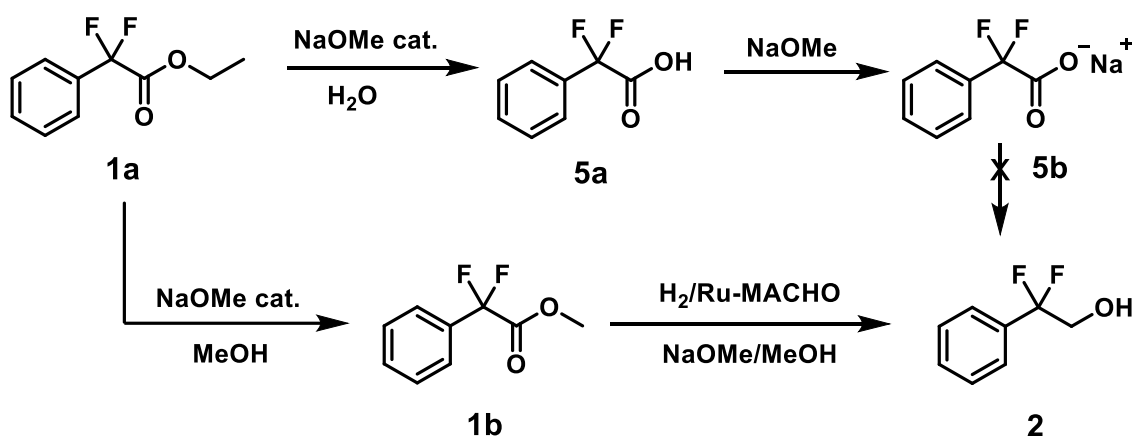
Figure 3.1.2: Comparison of ^1H -NMR spectra of Ru-MACHO-BH in DMSO-d_6 before and after exposure to air.

3.2. Translation of the Batch Protocol to Flow

3.2.1 Identification of the Side Product

From the initial batch optimisation experiments it was clear that a small amount of side product was always formed during the reaction. At this point the exact nature of the unwanted product was unknown. It was easily possible to show that the side product was caused by reaction with the added base sodium methoxide. By adding sodium methoxide to a solution of ethyl 2,2-difluoro-2-phenylacetate in methanol and analysing the resulting solution with ^{19}F -NMR, it was shown that small amounts of side product are formed quickly as soon as base is added. It was also possible to observe quick transesterification to the methyl ester **1b** as soon as base was added to the ethyl ester in methanolic solution.

By comparison of ^{19}F -NMR spectra of reaction solutions with spectra of the corresponding acid **5a** in basic methanolic solution the side product was identified as the deprotonated form of 2,2-difluoro-2-phenylacetic acid **5b**. The spectra used for the identification can be found in the appendix (Figure A1).



Scheme 3.2.1: Summary of side reactions that occur during the Ru-MACHO hydrogenation.

Scheme 3.2.1 shows the different pathways for side reactions in a representative reaction mixture for the Ru-MACHO hydrogenation. The transesterification of the ethyl ester **1a** to the methyl ester **1b** does not have an effect on the course of the reaction, because **1b** can be hydrogenated to product **2**. The saponification of ester **1a** to the acid **5a** followed by deprotonation by NaOMe to the sodium salt of the acid **5b** on the other hand is irreversible under basic conditions. Side product **5b** cannot react to form target product **2**. Additionally, the deprotonation of the acid leads to the consumption of NaOMe, which is needed to activate the catalyst Ru-MACHO. As a consequence of this side reaction, low base loadings can lead to reproducibility issues in the presence

of traces of water, because the base is consumed in the saponification. Another implication of the nature of the side reaction is that the side reaction can be limited by employing anhydrous conditions.

3.2.2 Optimisation in Flow

After good conditions for the performed reaction were found in the initial batch experiments the reaction was translated to continuous flow. Because of the known advantages for liquid-gas reactions under continuous flow conditions the reaction was expected to achieve similar or better results than in batch using a residence time of one hour or less.

As an initial starting point the centre conditions from the batch DoE were used. This decision was made, because the centre conditions showed full conversion and very good selectivity, as well as good reproducibility. Using higher catalyst loadings was not possible in flow, because of solubility issues with the catalyst.

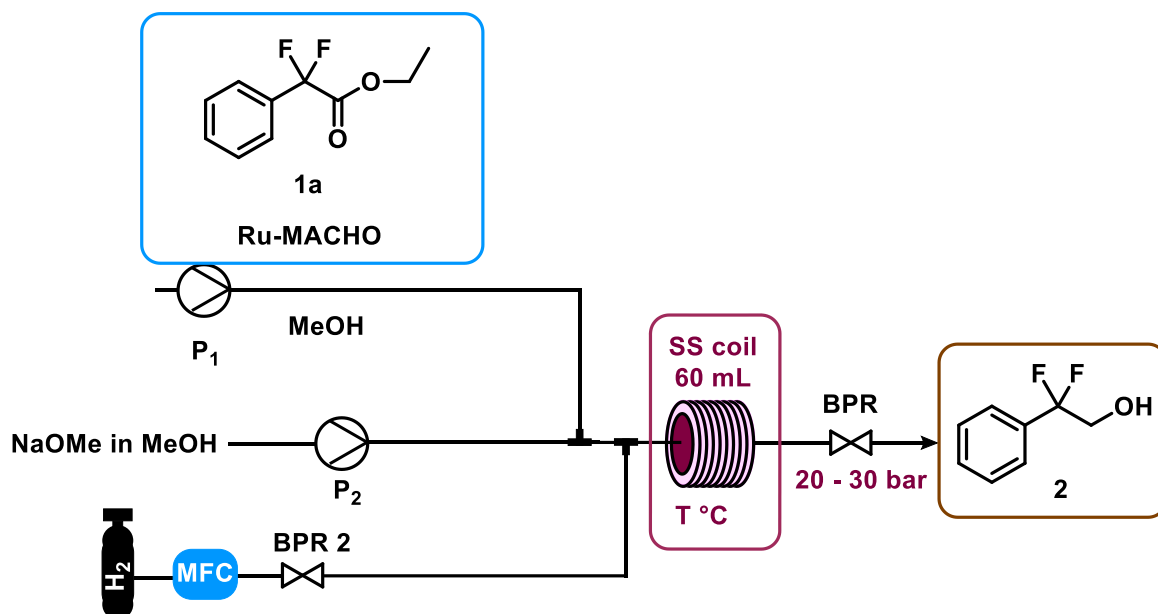


Figure 3.2.1: Flow scheme for the optimisation runs of the Ru-MACHO hydrogenation.

For flow experiments a setup using the Uniqsis FlowSyn system was used (Figure 3.2.1). The liquid phases were introduced in two different feeds. The base leads to the side reaction discussed in chapter 3.2.1 and the catalyst is known to decompose in the presence of base.^[80] To avoid any reaction in the feed solutions, the base was introduced separately from the catalyst and substrate. The two liquid feeds were introduced with HPLC pumps and H₂ was introduced through a mass flow controller (MFC). The two feeds were combined using a Y-shaped three-way mixer. A segmented

flow could be observed. The reaction was carried out in a 60 mL stainless steel coil and pressure was applied with a back-pressure regulator (BPR). Fractions were collected every 5 minutes and analysed using ^{19}F -NMR.

Table 3.2.1: First results of the batch optimisation.^[a]

Exp.	T [°C]	p [bar]	c [mol/L]	Base [eq.]	RT [min]	Conv. [%]	Product [%]
1	50	20	1.1	0.3	55	90	74
2	60	20	1	0.1	50	34	26
3a/3b ^[b]	60	20	1	0.1	50	80/9	73/0
4 ^[c]	60	20	1	0.1	50	50	40

^[a]0.4 mL/min total liquid flow rate, 30 mL_N/min H₂ flow rate, 0.065 mol% catalyst loading, total pumping time: 30 minutes. ^[b]Pre-stirring of base and catalyst for 15 minutes. ^[c]Pre-stirring of base and catalyst for 30 minutes.

Table 3.2.1 shows the results of the first optimisation attempts in flow. The first attempt at translating the batch conditions to flow showed high conversion but lower selectivity than expected (Exp. 1). Next the base loading was lowered, since the base loading was known to affect side product formation, but not product formation. Lowering the base loading to 0.1 equivalents unexpectedly decreased the conversion dramatically (Exp. 2).

To further mimic the conditions from the batch experiments, another setup was tried out. The base was pre-stirred with the catalyst and introduced in one feed, while the other feed just contained the substrate. The use of this setup with different times of pre-stirring (15 minutes: Exp. 3, 30 minutes: Exp. 4) led to irreproducible results. Operation under the exact same conditions (Exp. 3a and 3b) led to 73% of product and no conversion to product at all.

Table 3.2.2: Comparison of different reactor coil materials.^[a]

Coil	T [°C]	p [bar]	c [mol/L]	Base [eq.]	RT [min]	Conv. [%]	Product [%]
Stainless steel	50	20	1.1	0.3	55	90	74
PFA	50	20	1.1	0.3	60	97	86

^[a]0.4 mL/min total liquid flow rate, 30 mL_N/min H₂ flow rate, 0.065 mol% catalyst loading, total pumping time: 30 minutes.

To check for any influence of the stainless-steel reactor coil, the reaction was performed in a PFA coil of the same volume instead. Results from this comparison

reaction are shown in Table 3.2.2. The reaction showed similar results in PFA tubing than in stainless-steel. The increased conversion of the reaction in the polymer coil can be explained by slight residence time differences. It was concluded that the material of the coil had no significant impact on the reaction and was not causing the irreproducible results.

Table 3.2.3: Further optimisation and intensification.^[a]

Exp.	T [°C]	p [bar]	conc. [mol/L]	Base [eq.]	RT [min]	Conv. [%]	Product [%]
5a/5b	60	30	1	0.2	50-55	>99	91/93
6 ^[b]	60	30	1	0.2	50-55	>99	95
7 ^[b]	60	30	1.5	0.2	50-55	>99	96

^[a]0.4 mL/min total liquid flow rate, 45 mL_N/min H₂ flow rate, 0.065 mol% catalyst loading, total pumping time: 30 minutes. ^[b]Use of anhydrous methanol and fresh NaOMe solution, stored under Ar.

To finally achieve full conversion and reproducible results the base equivalents were increased to 0.2 eq. and the temperature and pressure were increased. With these conditions full conversion, over 90% of product and reproducible results were achieved (Table 3.2.3 exp. 5a/5b).

After the side product was identified it became clear that dry conditions would further improve the selectivity of the reaction. The use of dry methanol and a fresh bottle of NaOMe solution, which was stored under argon further increased the selectivity of the reaction under constant conditions (Table 3.2.3 exp. 6). It was also shown that an increase of the substrate concentration to 1.5 mol/L was possible without the loss of conversion or selectivity.

Unexpectedly, for all of the experiments, product was still found in the output stream of the reactor for far longer than expected. The product was still found in the output stream over an hour after the first product could be detected, even though the feeds were only introduced for 30 minutes during optimisation experiments. This led to the assumption that a lot of dispersion was happening, even though little to no dispersion would be expected for a gas-liquid reaction that shows slug flow.

To check for the influence of the used back pressure regulator (BPR), experiments using different BPRs were conducted. The use of a Zaiput BPR-10 did not lead to any significant improvement in the performance of the reaction, compared to the Swagelok BPR that was usually employed for the optimisation experiments. The use of a BPR by Chemtrix managed to solve the problems associated with dispersion and a broad residence time distribution. The broad residence time distribution was likely caused by back-mixing happening inside the internal volume of the BPRs. Since the BPR manufactured by Chemtrix has a much smaller internal volume than the BPR manufactured by Swagelok, much less dispersion was observed. Figure 3.2.2 shows a direct comparison of the course of the reaction under the same conditions using the different BPRs from Swagelok and Chemtrix. As expected, the conversion does not really change with the change of BPR. It is clearly visible that with the BPR by Chemtrix product stops coming out as expected around 30 minutes after the first residence time has passed. With the BPR by Swagelok on the other hand, product can be found in the reactor output tens of minutes later.

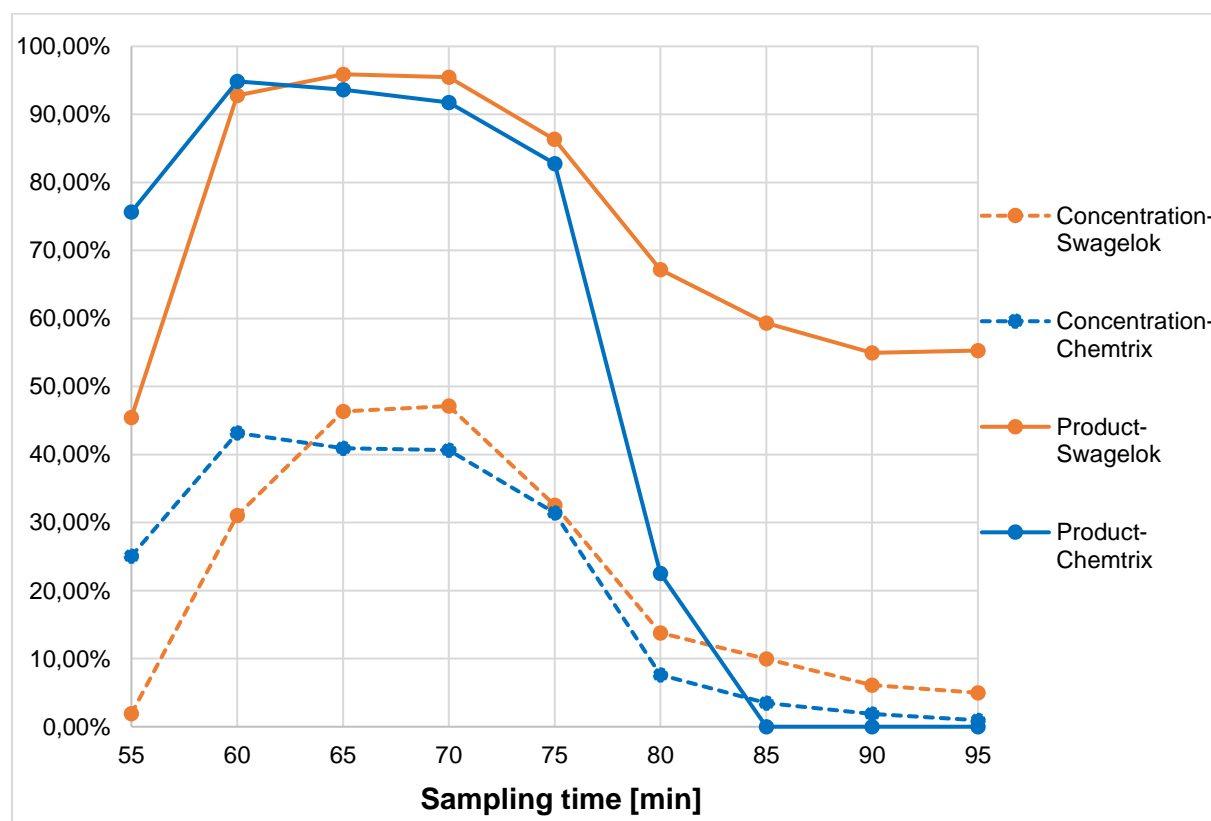


Figure 3.2.2: Comparison of concentration and amount of product in different fractions with two different BPRs. The concentration was estimated from a comparison to the internal standard.

3.2.3 Long Run

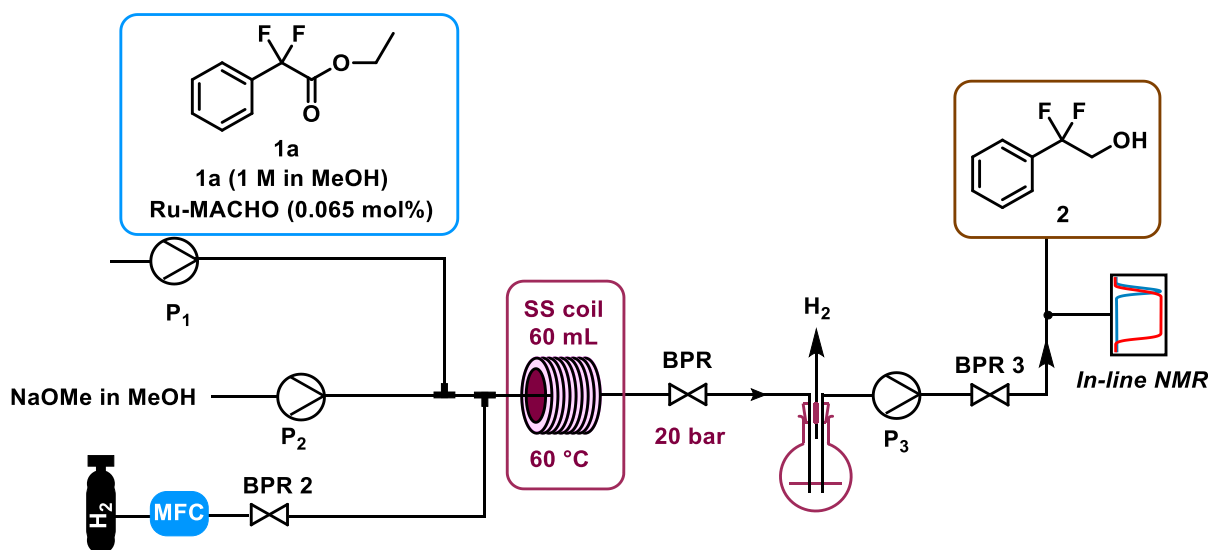


Figure 2.2.3: Flow scheme for the long run of the Ru-MACHO hydrogenation.

To check for long term stability of the reaction a long run was performed. The conditions that showed the most consistent output of reaction mixture, while maintaining high conversion and selectivity for the alcohol product were chosen for the long run (for details see chapter 5). The BPR manufactured by Chemtrix was used. Both feed solutions were set under argon atmosphere to avoid formation of the side product and to keep the conditions constant over the whole operation time. For the long run an in-line NMR measurement using a low-field benchtop NMR spectrometer was integrated into the setup downstream of the reactor (Figure 3.2.3). After separating the gas from the liquid stream, the reaction mixture was pumped through a flow cell inside a benchtop NMR spectrometer. This enabled the monitoring of the progress of the reaction in real time via ^{19}F -NMR spectroscopy. Otherwise the setup was kept the same from the optimisation runs.

Figure 3.2.4 shows the amount of product (P), starting material (SM) and side product (SP) as calculated by peak integration of the ^{19}F -NMR spectra from the in-line measurements. In addition, also data points for the amount of product in the collected fractions that were measured manually by ^{19}F -NMR are shown to validate the in-line measurement. Overall the reaction was operated at constant conditions for about 220 minutes, during which full conversion with 98% selectivity towards the target product could be observed. A throughput of 3.7 g/h was reached.

After combining the fractions from the constant operation time and a short extractive workup, the product could be obtained in 98% isolated yield (corresponding to the 220 minutes of constant conditions). Because of a slight pressure build up (from 20 to 22 bar) the output of reaction mixture was not completely stable at the beginning of the constant conditions. This leads to the assumption that the combined fractions that were worked up actually contained slightly more product than calculated. For this reason, the actual isolated yield should be slightly lower than the calculated 98%. If the yield is calculated for the full 240 minutes of operating time, an isolated yield of 90% is reached.

Overall it was shown that the reaction can be operated at constant conditions for 220 minutes without any decrease in conversion and selectivity.

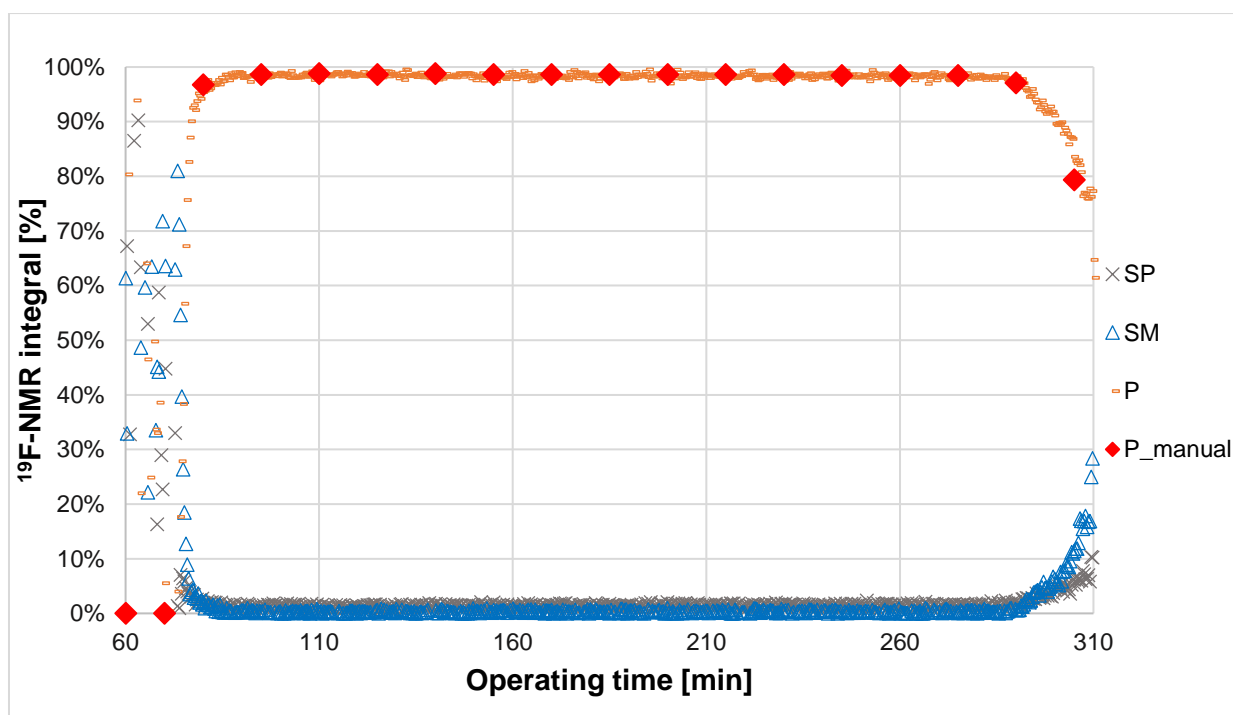
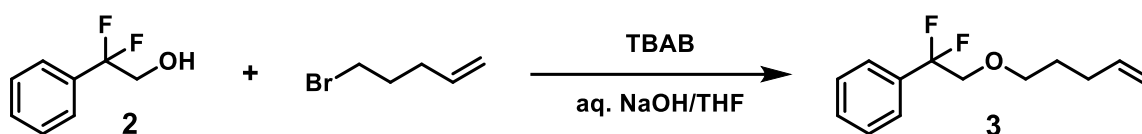


Figure 3.2.4: Composition of the reaction mixture over the operating time of the long run as determined by the in-line NMR measurement. The data points that are labelled P_manual are taken from manual measurements of all the fractions for validation.

3.3. Integrating the Ru-MACHO Hydrogenation into the Second Step



Scheme 3.3.1: PTC O-alkylation of 2,2-difluoro-2-phenylethanol **2** to product **3**.

To show that the product from the Ru-MACHO hydrogenation was viable to be taken onto the next step without any separation of catalyst residues, the next step in the reaction sequence was performed using product from the first step. The phase transfer catalysed (PTC) O-alkylation (Scheme 3.3.1) was performed using conditions previously optimised in our group for substrate produced by LAH reduction.

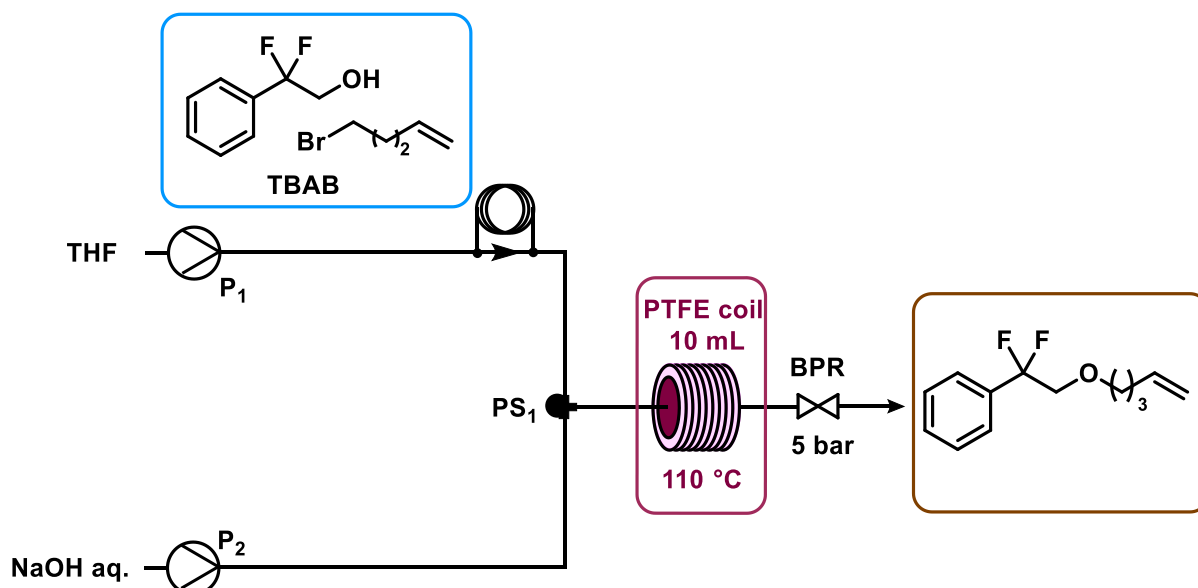


Figure 3.3.1: Flow scheme for the PTC O-Alkylation.

For flow experiments a setup using the Uniqsis FlowSyn system was used (Figure 3.3.1). The liquid phases were introduced in two different feeds. One HPLC pump was used to introduce the organic feed through a sample loop, while NaOH was pumped using a peristaltic pump (Vapourtec SF-10 reagent pump). The two feeds were combined using a Y-shaped three-way mixer. Solid formation was observed after mixing. After heating segmented flow could be observed. The reaction was carried out in a 10 mL PTFE coil and pressure was applied with a back-pressure regulator (Zaiput BPR-10). Fractions were collected every 5 minutes and the organic phase was analysed using ¹⁹F-NMR.

Table 3.3.1: Results of the O-alkylation reaction.^[a]

Entry	RT [min]	T [°C]	Flow rate [mL/min]	Alkene [eq.]	Conv. [%] ^[c]
1 ^[b]	23	110	0.5	1.05	>99
2	20	110	0.5	1.05	99 (90)
3	20	110	0.5	1.50	98 (94)
4	24	110	0.4	1.50	98 (96)

^[a]All reactions were performed with NaOH (aq. 40% w/w) and 0.9 M substrate in THF. ^[b]Reaction performed with 2,2-difluoro-2-phenylethanol, which was obtained from a LAH reduction. ^[c]Conversion determined by GC-FID, in brackets: conversion obtained by ¹⁹F-NMR peak integration.

Table 3.3.1 shows the results of the O-alkylation that was performed with product of the Ru-MACHO hydrogenation as substrate compared to results previously obtained with substrate obtained from a LAH reduction (entry 1). The residence time of the other reactions slightly differ from entry 1, because a new setup was used, with slightly different tubing lengths.

The results that were obtained show similarly high conversions of alcohol **2** to product **3** to the reaction with product from the LAH reduction. When measuring the conversion towards the target product **3** by GC-FID, all used conditions show close to full conversion. When using ¹⁹F-NMR for determining the conversion, all reactions show slightly lower conversion. The conversion is shown to be able to be increased by using higher equivalents of the alkene substrate or by increasing the residence time. It was concluded that the PTC O-alkylation reaction is not significantly influenced by the residual Ru-catalyst that remains in the isolated product of the Ru-MACHO hydrogenation reaction.

3.4 Comparison to the Currently Employed Route

3.4.1 Green Metrics

To determine how green the Ru-MACHO hydrogenation is compared to the LAH reduction a green metrics toolkit developed in 2015 by McElroy *et al* was used.^[44] In special the first pass toolkit, which was designed for promising laboratory scale reactions, was used to assess the old and new reaction.

Table 3.4.1 shows the results of the green metrics assessment for the newly employed Ru-MACHO catalysed reduction and for the LAH reduction employed in the current route. Both routes reach full conversion and good selectivity and yield, with the Ru-MACHO route reaching slightly higher values for the latter two values. The Ru-MACHO catalysed reaction shows better atom economy (AE) and reaction mass efficiency (RME) as well as higher optimum efficiency (OE). The process mass intensity (PMI) for the reaction is slightly lower for the Ru-MACHO reaction. Because of the catalytic nature of the Ru-MACHO reaction, no quenching of reagents is required. The simple extractive workup that is possible leads to a much lower total PMI than in the LAH reduction (PMI(Ru-MACHO) = 14.3, PMI(LAH) = 51.5).

Table 3.4.1 Results of the green assessment of the ester reduction steps from both routes.

Reaction	Conversion [%]	Selectivity [%]	Yield [%]	AE	RME	OE	PMI Reaction	PMI total
Ru-MACHO	>99	98	98	78.2	75.2	96.1	6.5	14.3
LAH ^[a]	>99	93	93	66.4	60.6	91.2	10.3	51.5

^[a]LAH reduction that is currently employed for the Abediterol synthesis.^[75]

Table 3.4.2 shows a short comparison of the two reductions concerning the qualitative green metrics that are applied. In the green metrics toolkit, coloured flags (green, amber, red) are given to each reaction to assess how green they are regarding each criterium. Green means “preferred”, amber “is acceptable-some issues” and red is “undesirable”. The Ru-MACHO reaction receives green flags for being catalytic and for being in flow. The LAH reduction on the other hand requires the stoichiometric use of LAH and is performed in batch, which results in two amber flags. Both reactions are operated in an energy efficient temperature window (0-70 °C) which results in green

flags. The LAH reduction takes place in THF at reflux conditions and is thus less energy efficient than the Ru-MACHO reaction, which is performed below reflux temperature. Because of the high amount of energy that is used when heating to reflux, this results in a red flag. The simple extractive workup of the RU-MACHO reaction also results in a green flag, while LAH requires a quench as well as extractions (amber flag).

The Ru-MACHO reaction only uses green solvents (methanol and ethyl acetate), while the LAH reduction also uses MTBE and THF which are considered of medium concern (amber flag). One drawback of the Ru-MACHO reaction is that ruthenium is considered a critical element, for which the supply could run out in the following 5-50 years (red flag). An additional amber flag is added because the catalyst is not currently recovered. Although the ruthenium catalyst can be employed at very low loadings (<0.1 mol%). The supply for lithium is predicted to be sufficient for 50-500 more years, which results in an amber flag.

Table 3.4.2: Comparison of qualitative green metrics of the Ru-MACHO hydrogenation and the LAH reduction.

Reaction	Type of reaction	T [°C]	Reflux	Workup	Solvents	Critical elements
Ru-MACHO	Catalytic/flow	60	No	Extraction	MeOH/ EtOAc/ Water	Ru
LAH	Stoichiometric/ batch	66	Yes	Quench & Extraction	THF/ Water/ MTBE	Li

3.4.2 Industrially and Economically Relevant Factors

Since the Ru-MACHO catalysed hydrogenation is set to be applied in the manufacturing of active pharmaceutical ingredients, it should be considered that limits for maximum contamination by metals have to be respected. Table 3.4.3 shows limits for some metals that are commonly used in catalysis in pharmaceuticals as calculated for healthy adults with 50 kg body weight.^[81]

Table 3.4.3: Limits of metals in pharmaceuticals

Metal	Oral Component limit (ppm)^[a]
Nickel	25
Palladium	10
Platinum	10
Osmium ^[b]	10
Rhodium ^[b]	10
Ruthenium ^[b]	10
Iridium ^[b]	10

^[a] assumes 10 g dose,

^[b] the sum of these metals should not exceed the displayed limits

For this reason, the residual metal from the catalyst has to be separated and possibly recycled at the end of the chemical synthesis. In 2015 the separation and recycling of homogeneous transition metal catalysts in continuous flow has been reviewed.^[82] For homogeneous catalysts methods such as the use of scavenging agents in solution or scavenging columns have been proposed. A short review on the removal of ruthenium after metathesis reactions has been published in 2012.^[83] The general methods that have been established for the removal of ruthenium can be split in two categories. The removal of homogeneous ruthenium catalysts by the use of scavengers and the immobilisation on heterogeneous support material. A sustainable method for the removal of ruthenium has been published in 2018.^[84] By addition of an isocyanide scavenger and treatment with acid, followed by a simple filtration, ruthenium levels below 5 ppm can be reached.

Table 3.4.4: Comparison of economically relevant factors between the LAH reduction and Ru-MACHO hydrogenation.

	LAH ^[a]	Ru-MACHO
Temperature [°C]	66	60
Reaction/Residence time [min]	60	60
Processing time [min]/ flow rate [mL/min]	60	0.4
Concentration [mol/L]	0.7	1
Reactor volume [ml]	250	60
Yield [g and g/h]	11.0	3.7
Space-time yield [kg/(m ³ ·min)]	0.73	1.04
Reagent per g of product [mg]	284.3	2.5
Metal per g of product [mg Li/Ru]	52.0	0.4
Price of reagent per g of product [€]	0.38 ^[b]	0.34 ^[c]

^[a]LAH reduction that is currently employed for the Abediterol synthesis.^[75] ^[b]Assuming 135 € for 100 g of LAH from Sigma Aldrich. ^[c]Assuming 134 € for 1 g of Ru-MACHO from Strem Chemicals.

Table 3.4.4 shows a comparison of economically relevant factors between the LAH reduction and the Ru-MACHO hydrogenation. The Ru-MACHO hydrogenation manages to achieve slightly higher space-time yield than the LAH reduction. Considering the catalytic nature of the Ru-MACHO hydrogenation, as expected, much lower amounts of the catalyst are required than LAH per gram of product. The price of the catalyst compared to the price of LAH per gram of product is very similar. In summary these factors indicate that the Ru-MACHO hydrogenation is economically competitive to the LAH reduction.

4. Conclusion and Outlook

In conclusion it was possible to optimise the reaction conditions for the Ru-MACHO catalysed hydrogenation of ethyl 2,2-difluoro-2-phenylacetate to the corresponding alcohol. This optimisation was achieved using a statistical design of experiments with a two-level full factorial design. Temperature, pressure and catalyst loading were shown to have a positive effect on the amount of product **2** generated. Base loading was shown to have a positive effect on the formation of the acid side **5b** product. Temperature and pressure were shown to have a negative effect on the formation of the acid side product. Using the optimum conditions full conversion and 96% selectivity towards the alcohol product was reached in only one hour of reaction time.

The reaction was successfully translated to continuous flow conditions. To our knowledge this is the first example of a homogeneously catalysed ester hydrogenation in flow. After further optimisation and intensification, the reaction showed full conversion and 96% selectivity after 50 minutes of residence time. It was possible to show that the reaction can be operated continuously at constant conditions for 220 minutes without any loss of yield. The reaction reached full conversion and excellent yield. After a simple extractive workup, the product could be isolated in excellent 98% yield, which corresponds to a throughput of 3.7 g/h.

It was possible to show that the reaction can be integrated into a new synthetic route for the lipophilic amine part of the drug Abediterol. Small amounts of residual Ru-catalyst were shown not to interfere with the second step of the API synthesis, which is a phase transfer catalysed O-alkylation.

Additionally, it has been shown that the Ru-MACHO catalysed hydrogenation leads to significantly improved green metrics, when compared to the LAH reduction which is usually applied. The catalytic hydrogenation reaches higher AE, RME and OE values and also a much lower total PMI value, when compared to the LAH reduction. It could also be shown that the Ru-MACHO reaction is economically competitive.

On the basis of this work and the optimisation of the rest of the newly modified route, future research should focus on fully integrating the steps into a telescoped synthesis. Additionally, strategies for removing and recycling the used ruthenium should be utilised to reduce the metal contamination to acceptable levels for the use in pharmaceuticals.

5. Experimental

5.1 General

Materials and Methods

Solvents and chemicals were obtained from commercial suppliers and were used without any further purification unless otherwise noted.

Design of Experiments (DoE)

The data for the batch optimisation was fitted in MODDE (version 11, Umetrics). The data that was measured in ^{19}F -NMR was fitted by using multiple linear regression (MLR) including main and interaction terms and then removing any terms where the contribution to the overall response was not significant.

High Field NMR

NMR spectra were recorded on a Bruker 300 MHz instrument. ^1H , ^{13}C and ^{19}F spectra were recorded at 300 MHz, 75 MHz and 282 MHz, respectively, with a chemical shift relative to tetramethylsilane (TMS) expressed in parts per million. Chemical shifts (δ) are reported in ppm downfield from TMS as the internal standard. The letters s, d, dd, t, tt, q, and m are used to indicate singlet, doublet, doublet of doublets, triplet, triplet of triplets, quadruplet, and multiplet respectively.

Benchtop NMR

In-Line NMR reaction monitoring was accomplished by recording ^{19}F spectra, using a low field benchtop 43 MHz NMR (Magritek, Spinsolve Ultra).

GC-FID

GC-FID analysis was performed on a ThermoFisher Focus GC with a flame ionization detector, using a TR-5MS column (30 m \times 0.25 mm ID \times 0.25 μm) and helium as carrier gas (1 mL \cdot min $^{-1}$ constant flow). The injector temperature was set to 280 $^{\circ}\text{C}$. After 1 min at 50 $^{\circ}\text{C}$, the temperature was increased by 25 $^{\circ}\text{C}\cdot$ min $^{-1}$ to 300 $^{\circ}\text{C}$ and kept constant at 300 $^{\circ}\text{C}$ for 4 min. The detector gases used for flame ionization were hydrogen and synthetic air (5.0 quality).

5.2 Batch Optimisation

5.2.1 Experiments using Ru-MACHO

To a 15 mL glass vial was added Ru-MACHO and methanol (2.5 mL). The resulting mixture was ultrasonicated until complete dissolution of the catalyst was reached. To the resulting solution were added ethyl 2,2-difluoro-2-phenylacetate (1 g, 5 mmol) and α,α,α -trifluorotoluene (73 mg, 0.5 mmol) as an internal standard. NaOMe was added as a solution in methanol (25% w/w). The content of the vial was transferred to a 25 mL HEL autoclave vessel containing a magnetic stirring bar. The vessel was flushed with nitrogen three times. It was heated and stirred at 600 rpm in a heating block for 10 minutes. The nitrogen atmosphere was replaced three times with hydrogen gas. The reaction was kept stirring at 600 rpm for 1 h in the heating block. The vessel was taken out of the heating block and cooled down in a water bath. The vessel was flushed three times with nitrogen and then opened. The reaction mixture was transferred to a fresh glass vial. Yield and selectivity of the reactions were determined using ^{19}F -NMR spectroscopy.

5.2.2 Experiments using Ru-MACHO-BH

A stock solution of Ru-MACHO-BH in methanol was prepared. Ru-MACHO-BH (57 mg, 97 μmol) was added to a 100 mL round bottom flask under glovebox conditions and sealed with a septum. The catalyst was dissolved in anhydrous methanol (50 mL) under ultrasonication.

To a 15 mL glass vial were added stock catalyst solution (2 mL, 3.8 μmol), ethyl 2,2-difluoro-2-phenylacetate (1 g, 5 mmol), α,α,α -trifluorotoluene (73 mg, 0.5 mmol) as internal standard and methanol (0.5 mL). NaOMe was added as a solution in methanol (25% w/w). The content of the vial was transferred to a 25 mL HEL autoclave vessel containing a magnetic stirring bar. The vessel was flushed with nitrogen three times. It was heated and stirred at 600 rpm in a heating block for 10 minutes. The nitrogen atmosphere was replaced three times with hydrogen gas. The reaction was kept stirring at 600 rpm for 1 h in the heating block. The vessel was taken out of the heating block and cooled down in a water bath. The vessel was flushed three times with nitrogen and then opened. The reaction mixture was transferred to a fresh glass vial. Yield and selectivity of the reactions were determined using ^{19}F -NMR spectroscopy.

5.3 Flow Procedure for the Optimisation Experiments

5.3.1 Feed Preparation

First feed: To a 10 mL volumetric flask was added NaOMe as a solution in methanol (25% w/w). Methanol was added to a total volume of 10 mL. The solution was transferred to a 15 mL glass vial.

Second feed: To a 5 mL volumetric flask was added Ru-MACHO, ethyl 2,2-difluoro-2-phenylacetate (3.2 g, 16 mmol) and α,α,α -trifluorotoluene (234 mg, 1.6 mmol) as internal standard. Methanol was added to a total volume of 5 mL. The resulting mixture was ultrasonicated until complete dissolution of the catalyst was reached. The solution was transferred to a 15 mL glass vial and 3 mL of methanol were added.

5.3.2 Flow Procedure

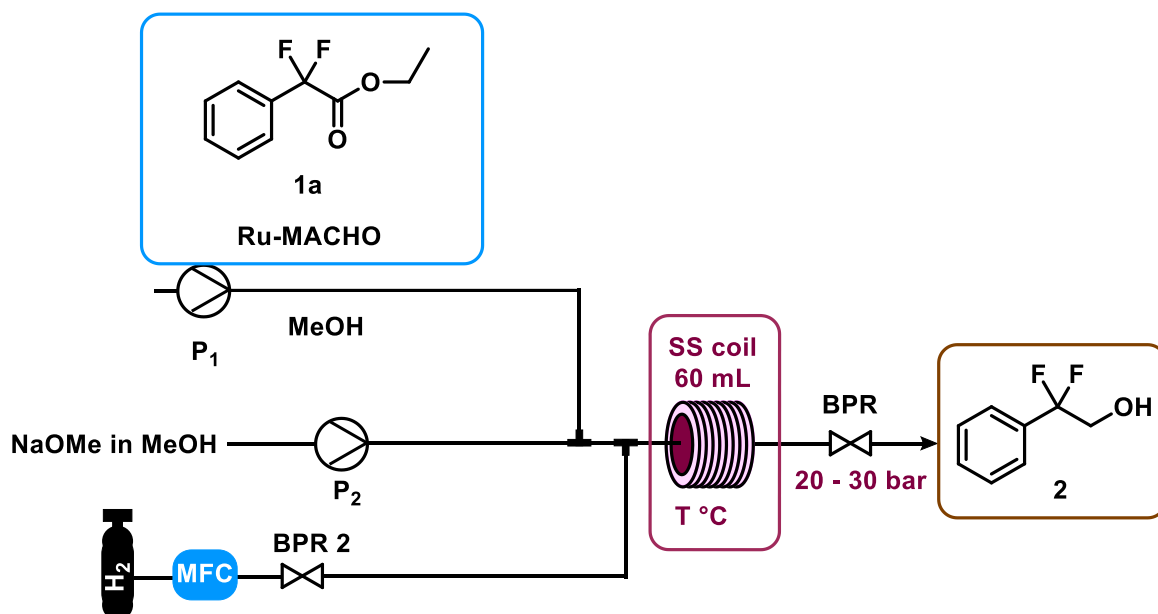


Figure 5.3.1: Flow scheme for the optimisation runs of the Ru-MACHO hydrogenation.

The flow setup (Figure 5.3.1) consisted of two high pressure liquid pumps (HPLC) (P₁, P₂, Uniqsis), for introducing the liquid feeds. H₂ gas was introduced from a gas cylinder using a calibrated mass flow controller (MFC, Bronkhorst-EL). The two liquid feeds were mixed in a mixer with integrated pressure sensor. The liquid stream was then combined with the gaseous stream using a Y-shaped three-way mixer. After the mixing a segmented flow regime could be observed. The mixer was connected to the reactor coil using fluoropolymer tubing (PFA, 0.8 mm inner diameter). For the reaction a 60 mL stainless steel coil on an aluminium heating block (Uniqsis FlowSyn) was used. After exiting the reaction coil the reaction mixture passed through a short piece of fluoropolymer tubing and an adjustable back pressure regulator (BPR, Swagelok 0-69

bar). A labelled picture of the setup is shown in Figure 5.3.2. Fractions of the liquid output were collected and used for analysis with ^{19}F -NMR. For optimisation experiments the liquid feed solutions were introduced for 30 minutes.

- A: Bronkhorst MFC
- B: Control Panel
- C: HPLC pumps (incorporated in FlowSyn)
- D: Y-shaped three-way connector
- E: SS reactor coil
- F: Swagelok BPR

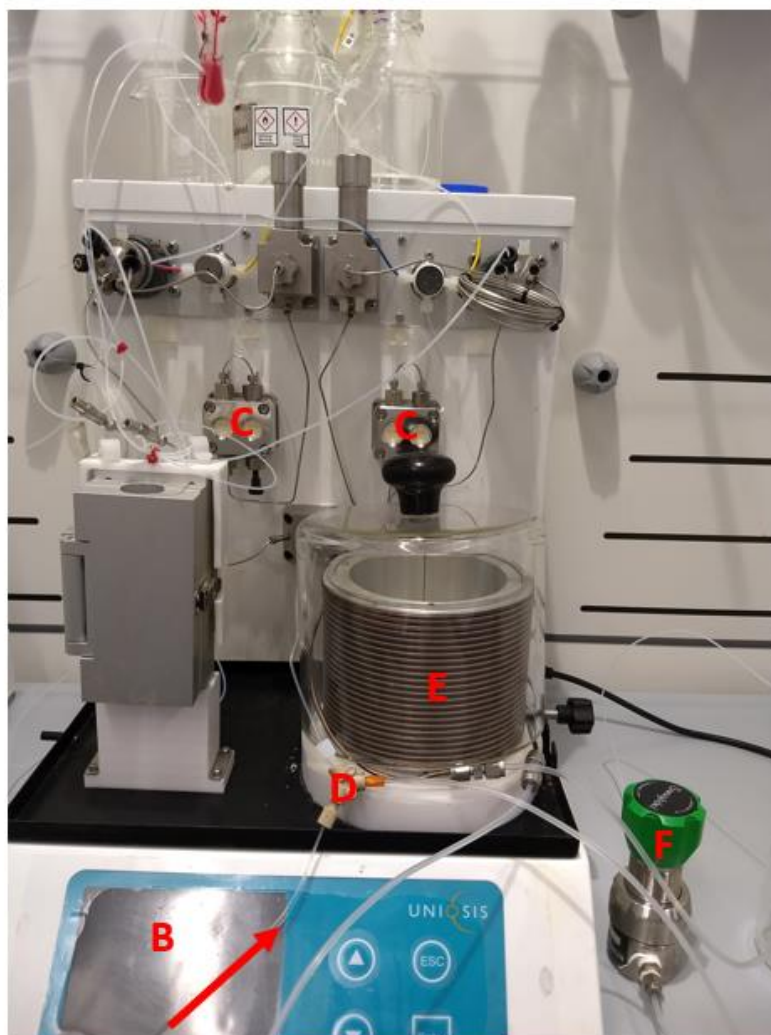


Figure 5.3.2: Labelled flow setup for the optimisation runs of the Ru-MACHO hydrogenation.

5.4 Flow Procedure for the Long Run

5.4.1 Feed Preparation

First feed: To a 50 mL volumetric flask was added NaOMe (1.31 g, 24.2 mmol) as a solution in methanol (25% w/w). Anhydrous methanol was added to a total volume of 50 mL. The feed solution was transferred to a 100 mL Duran bottle. Anhydrous methanol (10 mL) was added and the feed solution was set under argon atmosphere.

Second feed: To a 50 mL volumetric flask were added Ru-MACHO (47.5 mg, 78.2 μ mol), ethyl 2,2-difluoro-2-phenylacetate (24.02 g, 120.0 mmol) and α,α,α -trifluorotoluene (1.79 g, 12.3 mmol) as internal standard. Anhydrous methanol was added to a total volume of 50 mL and the solution was ultrasonicated until the catalyst was completely dissolved. The solution was transferred to a 100 mL Duran bottle. Anhydrous methanol (10 mL) was added and the feed solution was set under argon atmosphere.

5.4.2 Flow Procedure

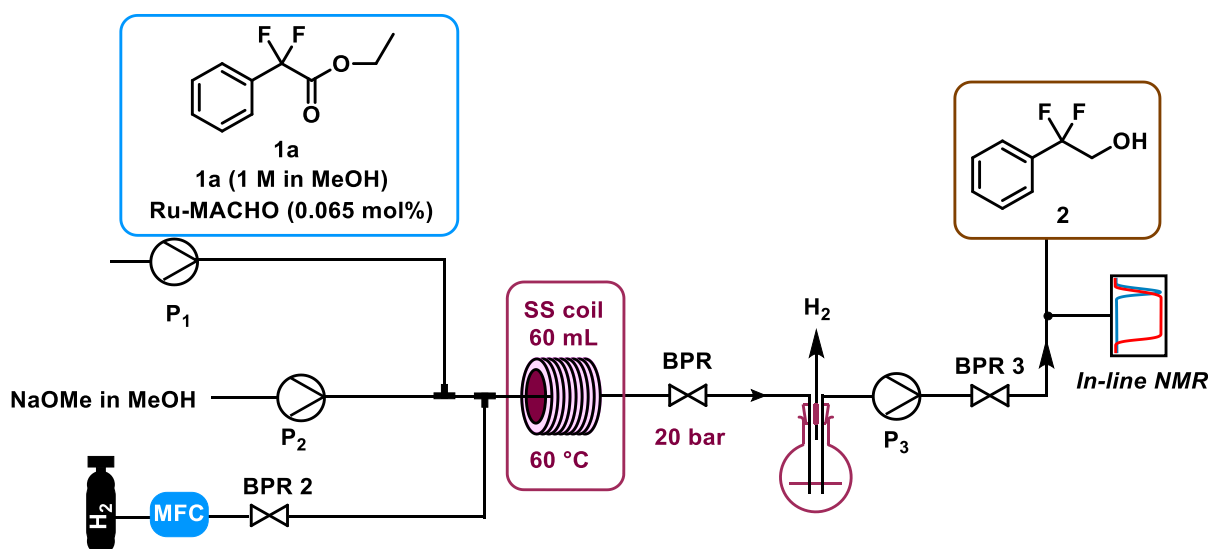


Figure 5.4.1: Flow scheme for the long run of the Ru-MACHO hydrogenation.

The flow setup (Figure 5.4.1) consisted of two high pressure liquid pumps (HPLC) (Uniqsis), for introducing the liquid feeds. H₂ gas was introduced from a gas cylinder using a calibrated mass flow controller (MFC, Bronkhorst-EL). The two liquid feeds were mixed in a mixer with integrated pressure sensor. The liquid stream was then combined with the gaseous stream using a Y-shaped three-way mixer. After the mixing a segmented flow regime could be observed. The mixer was connected to the reactor coil using fluoropolymer tubing (PFA, 0.8 mm inner diameter). For the reaction a 60 mL stainless steel coil on an aluminium heating block (Uniqsis FlowSyn) was used.

After exiting the reaction coil the reaction mixture passed through a short piece of fluoropolymer tubing and an adjustable back pressure regulator (BPR, Chemtrix, 0-20 bar). Afterwards the hydrogen was separated from the liquid phase in a glass vial. After this separation step the reaction mixture was continuously pumped through an NMR flow cell using a high-pressure liquid pump to measure in-line ^{19}F -NMR. A labelled picture of the setup is shown in Figure 5.4.2.

For the long run both feed solutions were introduced continuously for 4 hours. Conditions for the long run: 60°C, 20 bar, 0.2 mL/min liquid flow per pump, 30 mL_N/min H₂.

- A: Bronkhorst MFC
- B: Y-shaped three-way connector
- C: Control Panel
- D: SS reactor coil
- E: HPLC pumps (incorporated in FlowSyn)
- F: Feed solutions
- G: HPLC pump
- H: Chemtrix BPR
- I: Glass vial for gas separation
- J: BPR
- K: Benchtop NMR with flowcell



Figure 5.4.2: Labelled flow setup for the long run of the Ru-MACHO hydrogenation.

5.4.3 Workup

Fractions taken during steady state, corresponding to a total pumping time of 220 minutes (88 mL, 88 mmol of substrate) were combined into a 250 mL round bottom flask. The solvent was evaporated under vacuum. 50 mL of water were added and were extracted one time with 50 mL ethyl acetate and one time with 20 mL ethyl acetate. The combined organic phases were dried over Na₂SO₄ and filtered. The solvent was removed under vacuum to give an isolated yield of 13.69 g (86 mmol, 98% yield).

¹H-NMR (300.36 MHz, DMSO-d⁶): δ = 7.64 - 7.45 (m, 5H), δ = 5.78 - 5.68 (m, 1H), δ = 4.00 - 3.85 (m, 2H) ppm. ¹³C-NMR (75 MHz, DMSO-d⁶): δ = 135.2 (t, ²J_{CF} = 2 5.5 Hz), δ = 130.18 (s), δ = 128.54 (s), δ = 125.69 (t, ³J_{CF} = 6.2 Hz), δ = 121.62 (t, ¹J_{CF} = 242.8 Hz), δ = 64.27 (t, ²J_{CF} = 32.9 Hz) ppm. ¹⁹F-NMR (282 MHz, DMSO-d⁶): δ = -103.64 - -103.82 (m) ppm.

5.5 Phase-Transfer Catalysed O-Alkylation

5.5.1 Feed Preparation

First feed: To a 15 mL glass vial was added one equivalent of 2,2-difluoro-2-phenylethanol **2**. 5-bromo-1-pentene, tetrabutylammonium bromide (TBAB) and α,α,α -trifluorotoluene (10 mol%) as an internal standard were added. THF was added to form a homogeneous solution with a concentration of 0.9 mol/L of **2**.

Second feed: NaOH was slowly added to water under rigorous stirring and cooling with a water bath until a solution with a concentration of 40% w/w of NaOH was reached.

5.5.2 Flow Procedure

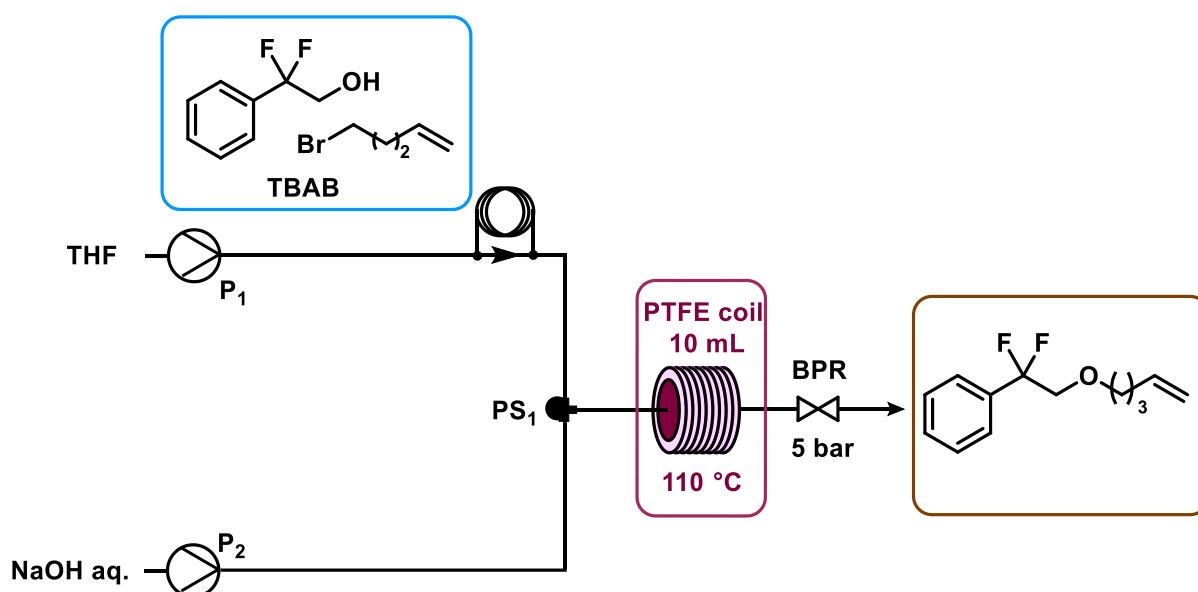


Figure 5.5.1: Flow scheme for the optimisation runs of the PTC O-alkylation.

The flow setup consisted of one high pressure liquid pump (HPLC) (P₁, Uniqsis), for introducing 2 mL of the first feed through sample loop injection. The second liquid feed was pumped directly through a peristaltic pump (Vapourtec SF-10 reagent pump, P₂). The two liquid feeds were mixed in a Y-shaped three-way mixer. After the mixing, solid formation was observed. After a higher temperature was reached a segmented flow regime could be observed. The mixer was connected to the reactor coil using fluoropolymer tubing (PFA, 0.8 mm inner diameter). For the reaction a 10 mL PTFE coil on an aluminium heating block (Uniqsis FlowSyn) was used. After exiting the reaction coil, the reaction mixture passed through a short piece of fluoropolymer tubing and an adjustable back pressure regulator (BPR, Zaiput BPR-10, 0-20 bar). A labelled picture of the setup is shown in Figure 5.5.2.

The organic phase of the collected biphasic mixture was used directly for analysis in ^{19}F -NMR and diluted 1:1000 for GC-FID analysis.

- A: HPLC pump
(incorporated in FlowSyn)**
- B: Injection loop**
- C: Vapourtec pump**
- D: Y-shaped three-way
connector**
- E: PTFE reactor coil**
- F: Zaiput BPR**
- G: Control Panel**



Figure 5.5.2: Labelled flow setup for the PTC O-alkylation.

References

- [1] I. J. Andersson, P.G., Munslow, *Modern Reduction Methods*, John Wiley & Sons, Weinheim, **2008**.
- [2] J. Seyden-Penne, *Reductions by the Alumino- and Borohydrides in Organic Synthesis*, **1997**.
- [3] I. Zakharin, LI, Khorlina, *Tetrahedron Lett.* **1962**, 619–620.
- [4] B. S. Bodnar, P. F. Vogt, *J. Org. Chem.* **2009**, *74*, 2598–2600.
- [5] J. An, D. N. Work, C. Kenyon, D. J. Procter, *J. Org. Chem.* **2014**, *79*, 6743–6747.
- [6] M. Han, X. Ma, S. Yao, Y. Ding, Z. Yan, A. Adijiang, Y. Wu, H. Li, Y. Zhang, P. Lei, et al., *J. Org. Chem.* **2017**, *82*, 1285–1290.
- [7] E. R. Burkhardt, K. Matos, *Chem. Rev.* **2006**, *106*, 2617–2650.
- [8] J. Pritchard, G. A. Filonenko, R. Van Putten, E. J. M. Hensen, E. A. Pidko, *Chem. Soc. Rev.* **2015**, *44*, 3808–3833.
- [9] H. Adkins, K. Folkers, *J. Am. Chem. Soc.* **1931**, *53*, 1095–1097.
- [10] H. Adkins, H. I. Cramer, R. Connor, *J. Am. Chem. Soc.* **1931**, *53*, 1402–1405.
- [11] K. Folkers, H. Adkins, *J. Am. Chem. Soc.* **1932**, *54*, 1145–1154.
- [12] R. Connor, K. Folkers, H. Adkins, *J. Am. Chem. Soc.* **1932**, *54*, 1138–1145.
- [13] D. S. Thakur, B. D. Roberts, T. J. Sullivan, A. L. Vichok, *US Patent*, **1992**, 5,155,086.
- [14] U. R. Kreutzer, *J. Am. Oil Chem. Soc.* **1984**, *61*, 343–348.
- [15] Y. Pouilloux, F. Autin, J. Barrault, *Catal. Today* **2000**, *63*, 87–100.
- [16] J. Zheng, H. Lin, Y. N. Wang, X. Zheng, X. Duan, Y. Yuan, *J. Catal.* **2013**, *297*, 110–118.
- [17] J. C. R. A. Grey, G. P. Pez, A. Wallo, *Chem. Commun.* **1980**, 783–784.
- [18] G. P. Pez, R. A. Grey, J. Corsi, *J. Am. Chem. Soc.* **1981**, *103*, 7528–7535.
- [19] R. A. Grey, G. P. Pez, A. Wallo, *J. Am. Chem. Soc.* **1981**, *103*, 7536–7542.

- [20] U. Matteoli, G. Menchi, M. Bianchi, F. Piacenti, *J. Organomet. Chem.* **1986**, 299, 233–238.
- [21] H. T. Teunissen, C. J. Elsevier, *Chem. Commun.* **1997**, 667–668.
- [22] H. T. Teunissen, C. J. Elsevier, *Chem. Commun.* **1998**, 3, 1367–1368.
- [23] J. Zhang, G. Leitun, Y. Ben-David, D. Milstein, *Angew. Chemie - Int. Ed.* **2006**, 45, 1113–1115.
- [24] L. A. Saudan, C. M. Saudan, C. Debieux, P. Wyss, *Angew. Chemie - Int. Ed.* **2007**, 46, 7473–7476.
- [25] W. Kuriyama, T. Matsumoto, O. Ogata, Y. Ino, K. Aoki, S. Tanaka, K. Ishida, T. Kobayashi, N. Sayo, T. Saito, *Org. Process Res. Dev.* **2012**, 16, 166–171.
- [26] D. Spasyuk, S. Smith, D. G. Gusev, *Angew. Chemie - Int. Ed.* **2012**, 51, 2772–2775.
- [27] D. Spasyuk, S. Smith, D. G. Gusev, *Angew. Chemie - Int. Ed.* **2013**, 52, 2538–2542.
- [28] T. Zell, Y. Ben-David, D. Milstein, *Angew. Chemie - Int. Ed.* **2014**, 53, 4685–4689.
- [29] S. Chakraborty, H. Dai, P. Bhattacharya, N. T. Fairweather, M. S. Gibson, J. A. Krause, H. Guan, *J. Am. Chem. Soc.* **2014**, 136, 7869–7872.
- [30] K. Junge, B. Wendt, H. Jiao, M. Beller, *ChemCatChem* **2014**, 6, 2810–2814.
- [31] S. Elangovan, M. Garbe, H. Jiao, A. Spannenberg, K. Junge, M. Beller, *Angew. Chemie* **2016**, 128, 15590–15594.
- [32] N. A. Espinosa-Jalapa, A. Nerush, L. J. W. Shimon, G. Leitun, L. Avram, Y. Ben-David, D. Milstein, *Chem. - A Eur. J.* **2017**, 23, 5934–5938.
- [33] D. Srimani, A. Mukherjee, A. F. G. Goldberg, G. Leitun, Y. Diskin-Posner, L. J. W. Shimon, Y. Ben David, D. Milstein, *Angew. Chemie Int. Ed.* **2015**, 54, 12357–12360.
- [34] T. J. Korstanje, J. Ivar van der Vlugt, C. J. Elsevier, B. de Bruin, *Science* **2015**, 350, 298–302.

- [35] T. Otsuka, A. Ishii, P. A. Dub, T. Ikariya, *J. Am. Chem. Soc.* **2013**, *135*, 9600–9603.
- [36] J. C. Anastas, P. T.; Warner, *Green Chemistry: Theory and Practice*, Oxford University Press, New York, **1998**.
- [37] P. T. Anastas, J. B. Zimmerman, *IEEE Eng. Manag. Rev.* **2007**, *35*, 16.
- [38] M. A. Abraham, N. Nguyen, *Environ. Prog.* **2003**, *22*, 233–236.
- [39] J. Andraos, *Org. Process Res. Dev.* **2005**, *9*, 149–163.
- [40] B. Trost, *Science* **1991**, *254*, 1471–1477.
- [41] A. Sheldon, Roger, *Chem. Ind.* **1992**, *23*, 903–6.
- [42] A. D. Curzons, D. J. C. Constable, D. N. Mortimer, V. L. Cunningham, *Green Chem.* **2001**, *3*, 1–6.
- [43] C. Jimenez-Gonzalez, C. S. Ponder, Q. B. Broxterman, J. B. Manley, *Org. Process Res. Dev.* **2011**, *15*, 912–917.
- [44] C. R. McElroy, A. Constantinou, L. C. Jones, L. Summerton, J. H. Clark, *Green Chem.* **2015**, *17*, 3111–3121.
- [45] B. Gutmann, D. Cantillo, C. O. Kappe, *Angew. Chemie - Int. Ed.* **2015**, *54*, 6688–6728.
- [46] M. Movsisyan, E. I. P. Delbeke, J. K. E. T. Berton, C. Battilocchio, S. V. Ley, C. V. Stevens, *Chem. Soc. Rev.* **2016**, *45*, 4892–4928.
- [47] M. B. Plutschack, B. Pieber, K. Gilmore, P. H. Seeberger, *Chem. Rev.* **2017**, *117*, 11796–11893.
- [48] C. J. Mallia, I. R. Baxendale, *Org. Process Res. Dev.* **2016**, *20*, 327–360.
- [49] D. Dallinger, C. O. Kappe, *Curr. Opin. Green Sustain. Chem.* **2017**, *7*, 6–12.
- [50] J. I. Yoshida, H. Kim, A. Nagaki, *ChemSusChem* **2011**, *4*, 331–340.
- [51] V. Hessel, D. Kralisch, N. Kockmann, T. Noël, Q. Wang, *ChemSusChem* **2013**, *6*, 746–789.
- [52] C. F. Carter, H. Lange, S. V. Ley, I. R. Baxendale, B. Wittkamp, J. G. Goode, N. L. Gaunt, *Org. Process Res. Dev.* **2010**, *14*, 393–404.

- [53] S. A. Leung, R. F. Winkle, R. C. R. Wootton, A. J. DeMello, *Analyst* **2005**, *130*, 46–51.
- [54] F. Benito-Lopez, W. Verboom, M. Kakuta, J. G. E. Gardeniers, R. J. M. Egberink, E. R. Oosterbroek, A. Van Den Berg, D. N. Reinhoudt, *Chem. Commun.* **2005**, 2857–2859.
- [55] P. Giraudeau, F. X. Felpin, *React. Chem. Eng.* **2018**, *3*, 399–413.
- [56] D. L. Browne, S. Wright, B. J. Deadman, S. Dunnage, I. R. Baxendale, R. M. Turner, S. V. Ley, *Rapid Commun. Mass Spectrom.* **2012**, *26*, 1999–2010.
- [57] D. L. Riley, N. C. Neyt, *Synth.* **2018**, *50*, 2707–2720.
- [58] D. Mandala, S. Chada, P. Watts, *Org. Biomol. Chem.* **2017**, *15*, 3444–3454.
- [59] L. Ducry, D. M. Roberge, *Org. Process Res. Dev.* **2008**, *12*, 163–167.
- [60] D. Webb, T. F. Jamison, *Org. Lett.* **2012**, *14*, 568–571.
- [61] M. Yoshida, H. Otaka, T. Doi, *European J. Org. Chem.* **2014**, *2014*, 6010–6016.
- [62] T. Fukuyama, H. Chiba, H. Kuroda, T. Takigawa, A. Kayano, K. Tagami, *Org. Process Res. Dev.* **2016**, *20*, 503–509.
- [63] J. M. De Muñoz, J. Alcázar, A. De La Hoz, A. Díaz-Ortiz, *European J. Org. Chem.* **2012**, 260–263.
- [64] C. O. Ötvös, Sándor B., Kappe, *ChemSusChem* **2020**, *Accepted M*, DOI 10.1002/cssc.201903459.
- [65] R. A. Fisher, *The Design of Experiments*, Hafner Publishing Company, New York, **1966**.
- [66] R. A. Fisher, *Statistical Methods for Research Workers*, Oliver And Boyd, Edinburgh; London, **1970**.
- [67] A. Gioiello, V. Mancino, P. Filippini, S. Mostarda, B. Cerra, *J. Flow Chem.* **2016**, *6*, 167–180.
- [68] S. A. Weissman, N. G. Anderson, *Org. Process Res. Dev.* **2015**, *19*, 1605–1633.
- [69] G. P. Taber, D. M. Pfisterer, J. C. Colberg, *Org. Process Res. Dev.* **2004**, *8*, 385–388.

- [70] R. Leardi, *Anal. Chim. Acta* **2009**, *652*, 161–172.
- [71] M. R. Owen, C. Luscombe, L. W. Lai, S. Godbert, D. L. Crookes, D. Emiabata-Smith, *Org. Process Res. Dev.* **2001**, *5*, 308–323.
- [72] M. Aparici, M. Gómez-Angelats, D. Vilella, R. Otal, C. Carcasona, M. Viñals, I. Ramos, A. Gavaldà, J. De Alba, J. Gras, et al., *J. Pharmacol. Exp. Ther.* **2012**, *342*, 497–509.
- [73] W. Timmer, E. Massana, E. Jimenez, B. Seoane, G. de Miquel, S. Ruiz, *J. Clin. Pharmacol.* **2014**, *54*, 1347–1353.
- [74] J. Beier, R. Fuhr, E. Massana, E. Jiménez, B. Seoane, G. De Miquel, S. Ruiz, *Respir. Med.* **2014**, *108*, 1424–1429.
- [75] R. H. Munday, L. Goodman, G. M. Noonan, *Tetrahedron Lett.* **2019**, *60*, 606–609.
- [76] D. De Zani, M. Colombo, *J. Flow Chem.* **2012**, *2*, 5–7.
- [77] B. Reichart, C. O. Kappe, T. N. Glasnov, *Synlett* **2013**, *24*, 2393–2396.
- [78] X. Wang, *J. Flow Chem.* **2015**, *5*, 125–132.
- [79] J. Gallardo-Donaire, M. Ernst, O. Trapp, T. Schaub, *Adv. Synth. Catal.* **2016**, *358*, 358–363.
- [80] A. Anaby, M. Schelwies, J. Schwaben, F. Rominger, A. S. K. Hashmi, T. Schaub, *Organometallics* **2018**, *37*, 2193–2201.
- [81] D. R. Abernethy, A. J. DeStefano, T. L. Cecil, K. Zaidi, R. L. Williams, *Pharm. Res.* **2010**, *27*, 750–755.
- [82] I. Vural Gürsel, T. Noël, Q. Wang, V. Hessel, *Green Chem.* **2015**, *17*, 2012–2026.
- [83] G. C. Vougioukalakis, *Chem. - A Eur. J.* **2012**, *18*, 8868–8880.
- [84] G. Szczepaniak, A. Ruszczyńska, K. Kosiński, E. Bulska, K. Grela, *Green Chem.* **2018**, *20*, 1280–1289.

Appendix

Table A1: Conditions for the experiments included in the two-level full factorial design.

No.	Pressure [bar]	Temperature [°C]	Catalyst [mol%]	Base [eq.]
1	10	40	0.03	0.1
2	30	40	0.03	0.1
3	10	60	0.03	0.1
4	30	60	0.03	0.1
5	10	40	0.1	0.1
6	30	40	0.1	0.1
7	10	60	0.1	0.1
8	30	60	0.1	0.1
9	10	40	0.03	0.3
10	30	40	0.03	0.3
11	10	60	0.03	0.3
12	30	60	0.03	0.3
13	10	40	0.1	0.3
14	30	40	0.1	0.3
15	10	60	0.1	0.3
16	30	60	0.1	0.3
17	20	50	0.065	0.2
18	20	50	0.065	0.2
19	20	50	0.065	0.2

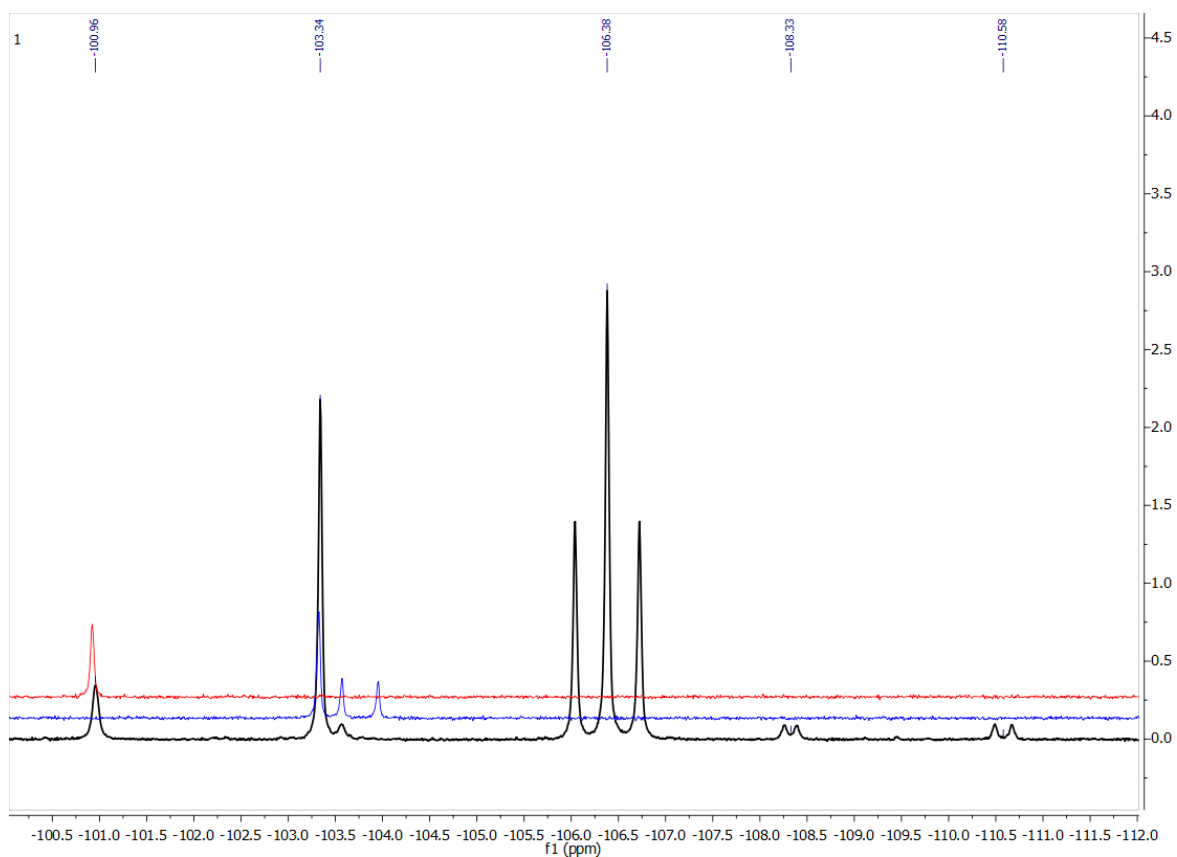


Figure A1: ^{19}F -NMR to elucidate the side product: The black spectrum shows a representative spectrum of a reaction mixture. The blue spectrum shows the methyl and ethyl ester (**1a** and **1b**) and the corresponding acid (**5a**). The red spectrum shows the acid (**5a**) in basic methanol solution, which overlaps with the peak corresponding with the side product in black at -100.96 ppm.

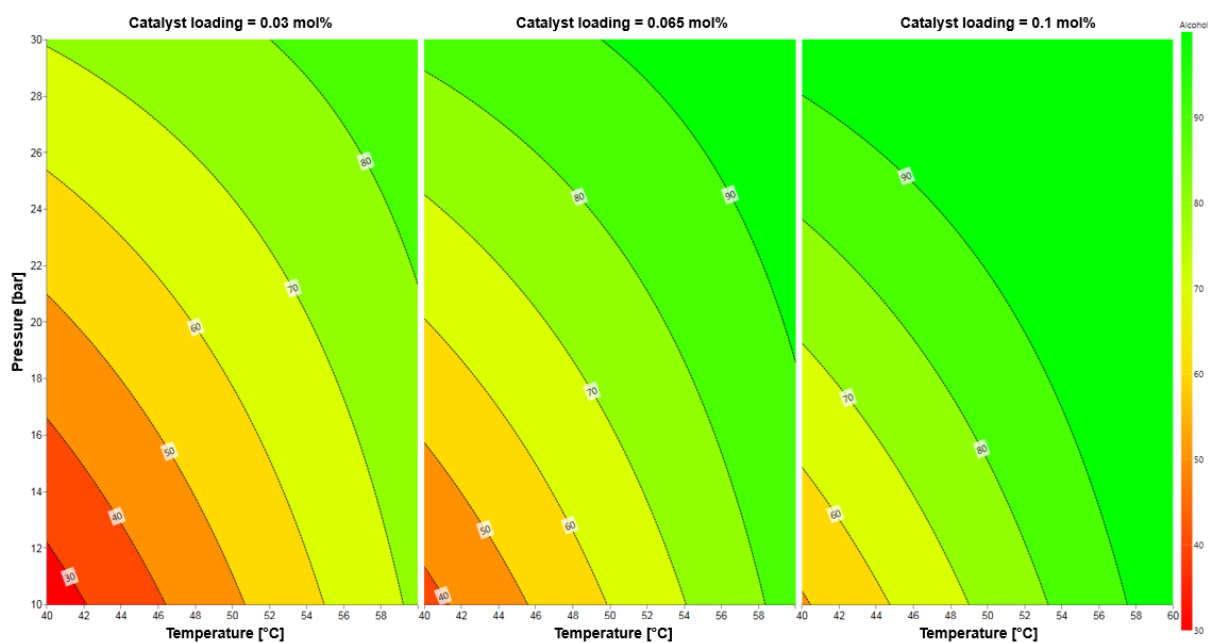


Figure A2: Contour plots comparing different conditions for pressure, temperature and catalyst loading regarding their influence on the formation of alcohol product **2**.

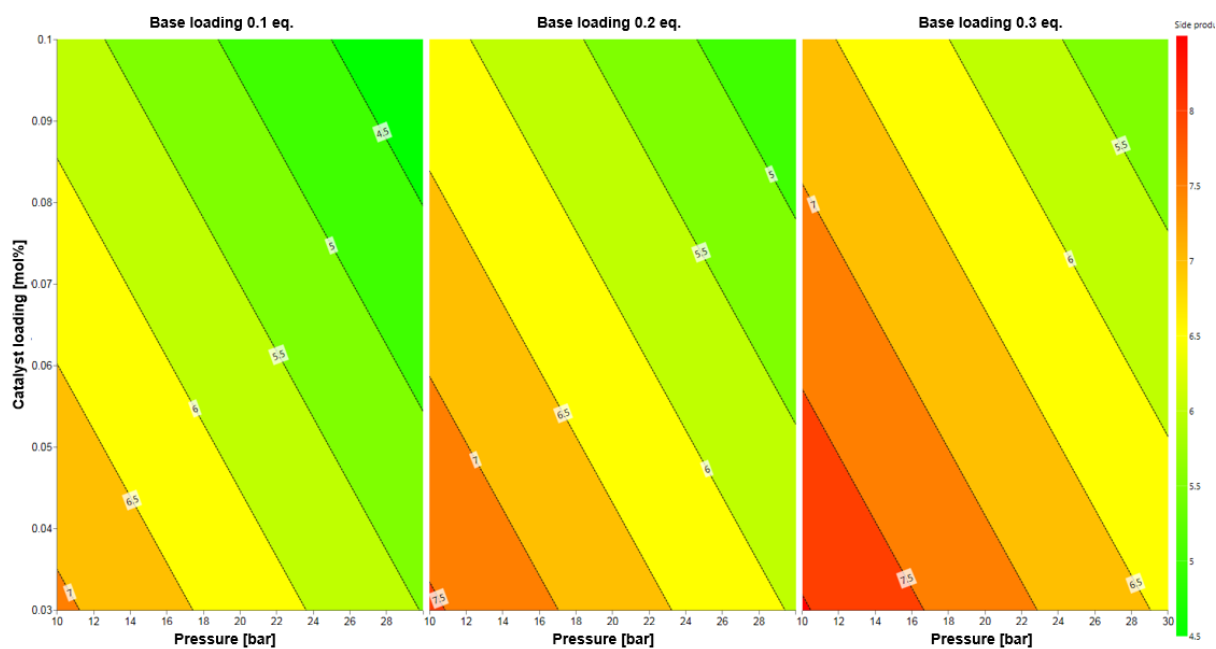


Figure A3: Contour Plots comparing different conditions for catalyst loading, pressure and base loading regarding their influence on the formation of side product **5b**.

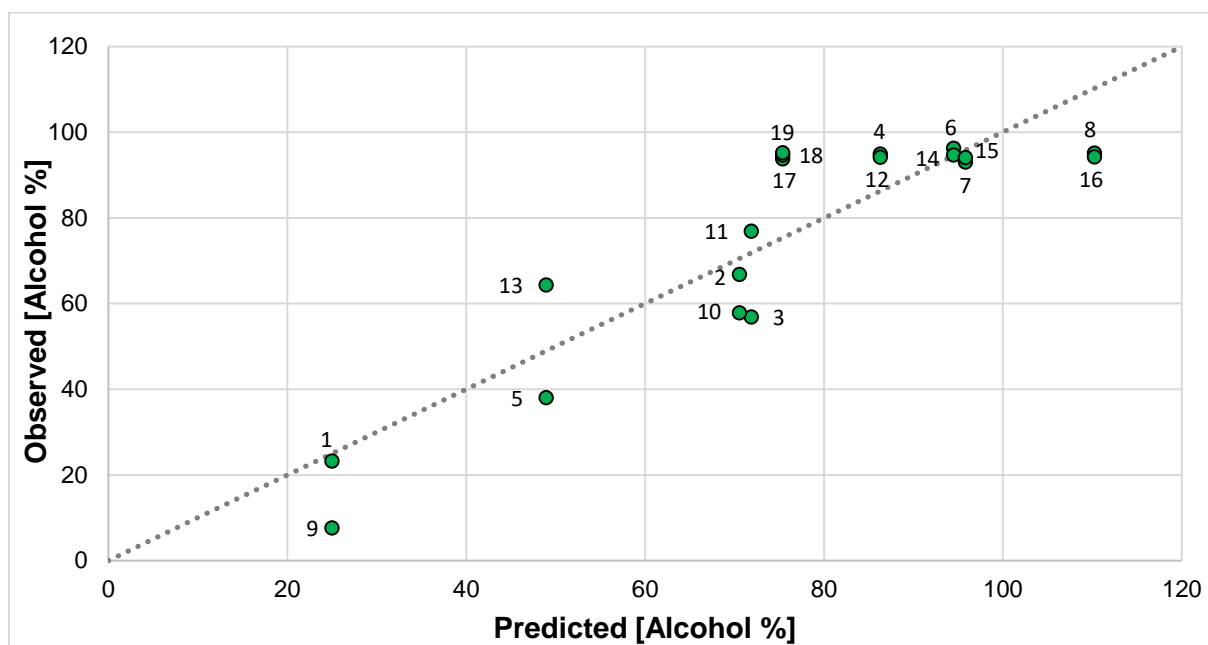


Figure A4: Observed values for the % of generated alcohol product **2** versus the predicted values by the multiple linear regression model.

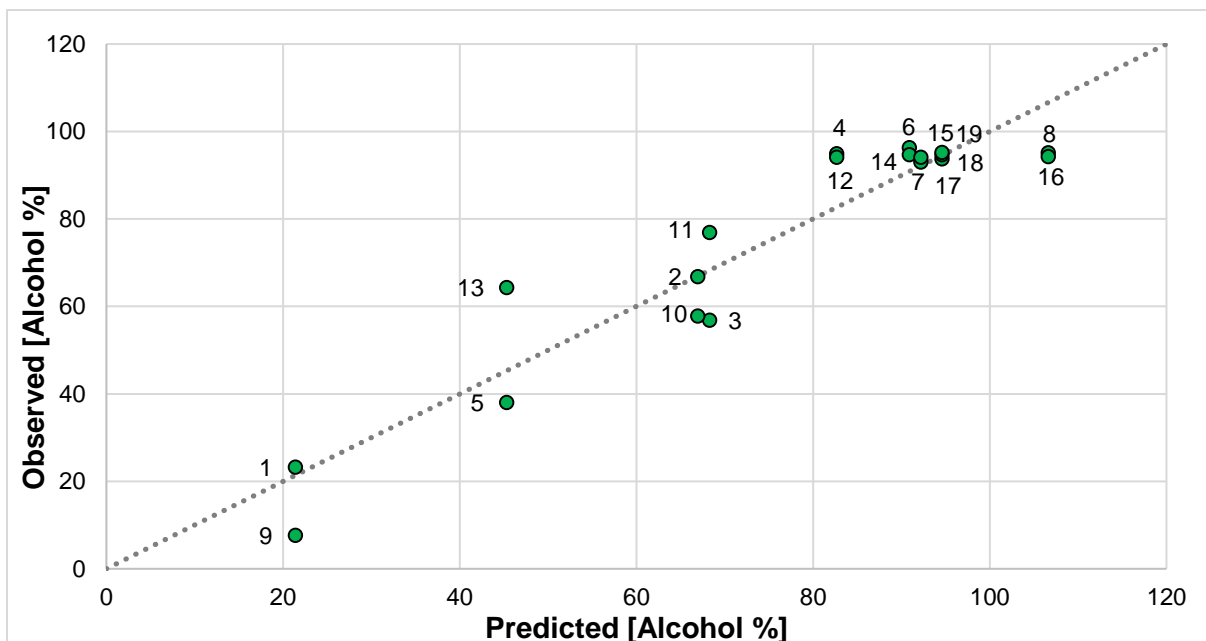


Figure A5: Observed values for the % of generated alcohol product 2 versus the predicted values by the model including square terms.

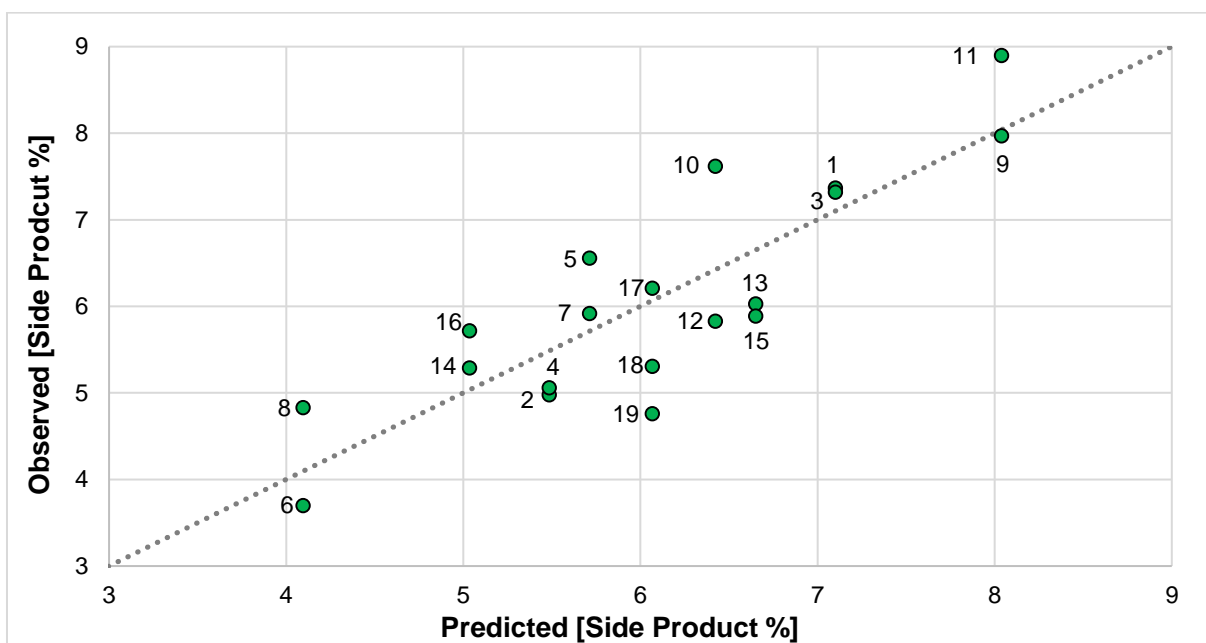


Figure A6: Observed values for the % of generated side product 5b versus the predicted values by the multiple linear regression model.

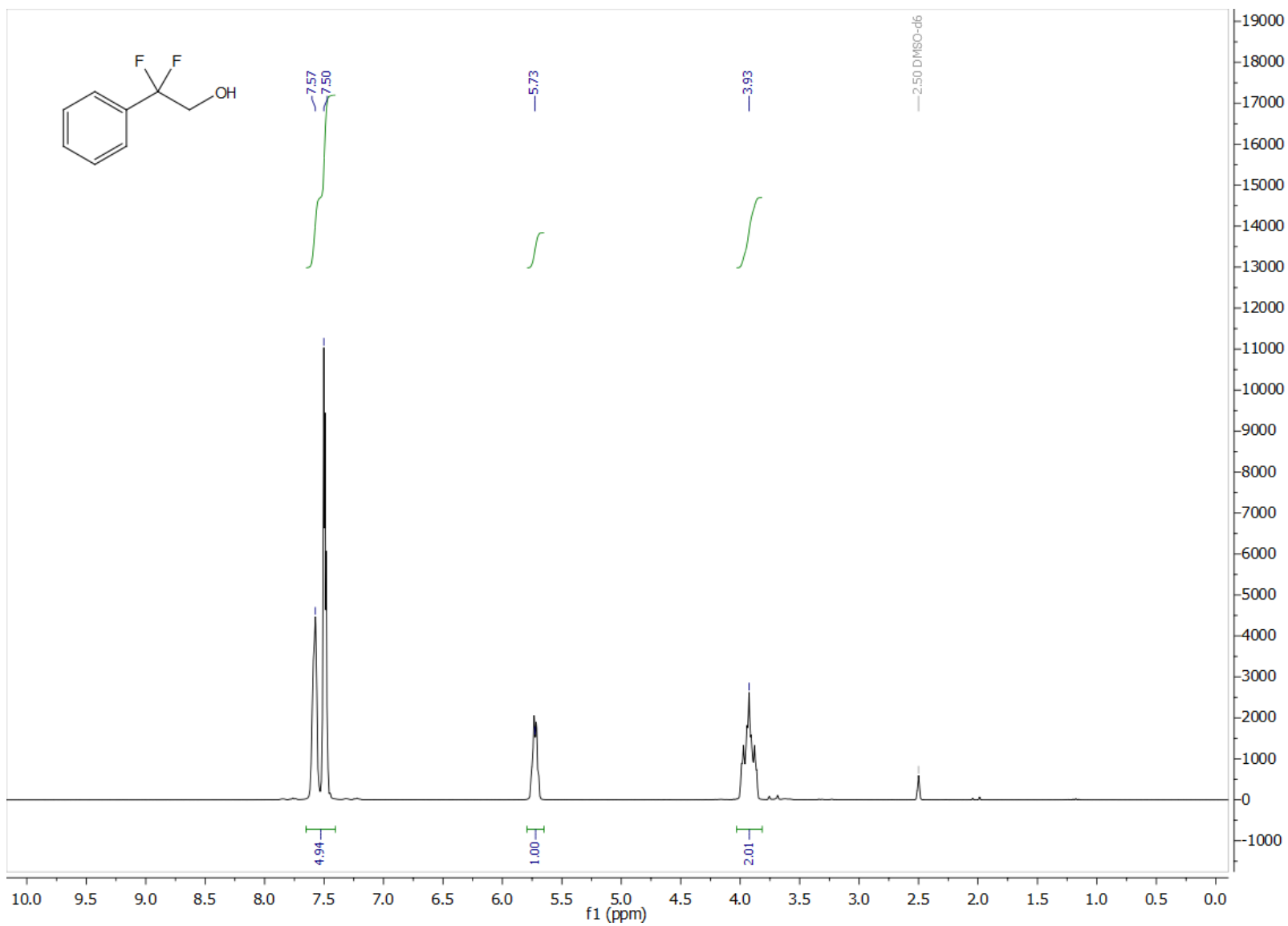


Figure A7: $^1\text{H-NMR}$ spectrum of 2,2-difluoro-2-phenylethanol **2**.

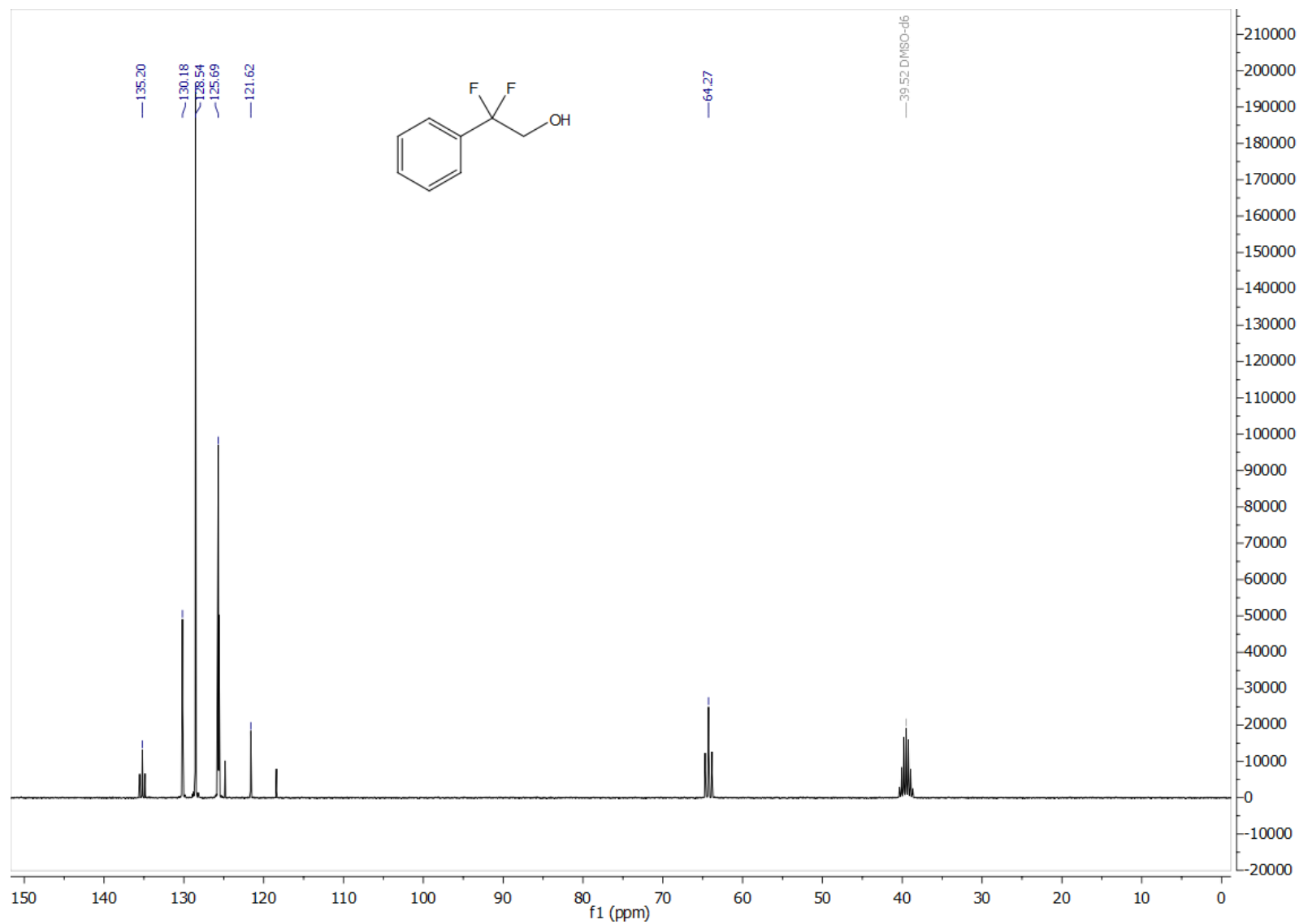


Figure A8: ^{13}C -NMR spectrum of 2,2-difluoro-2-phenylethanol **2**.

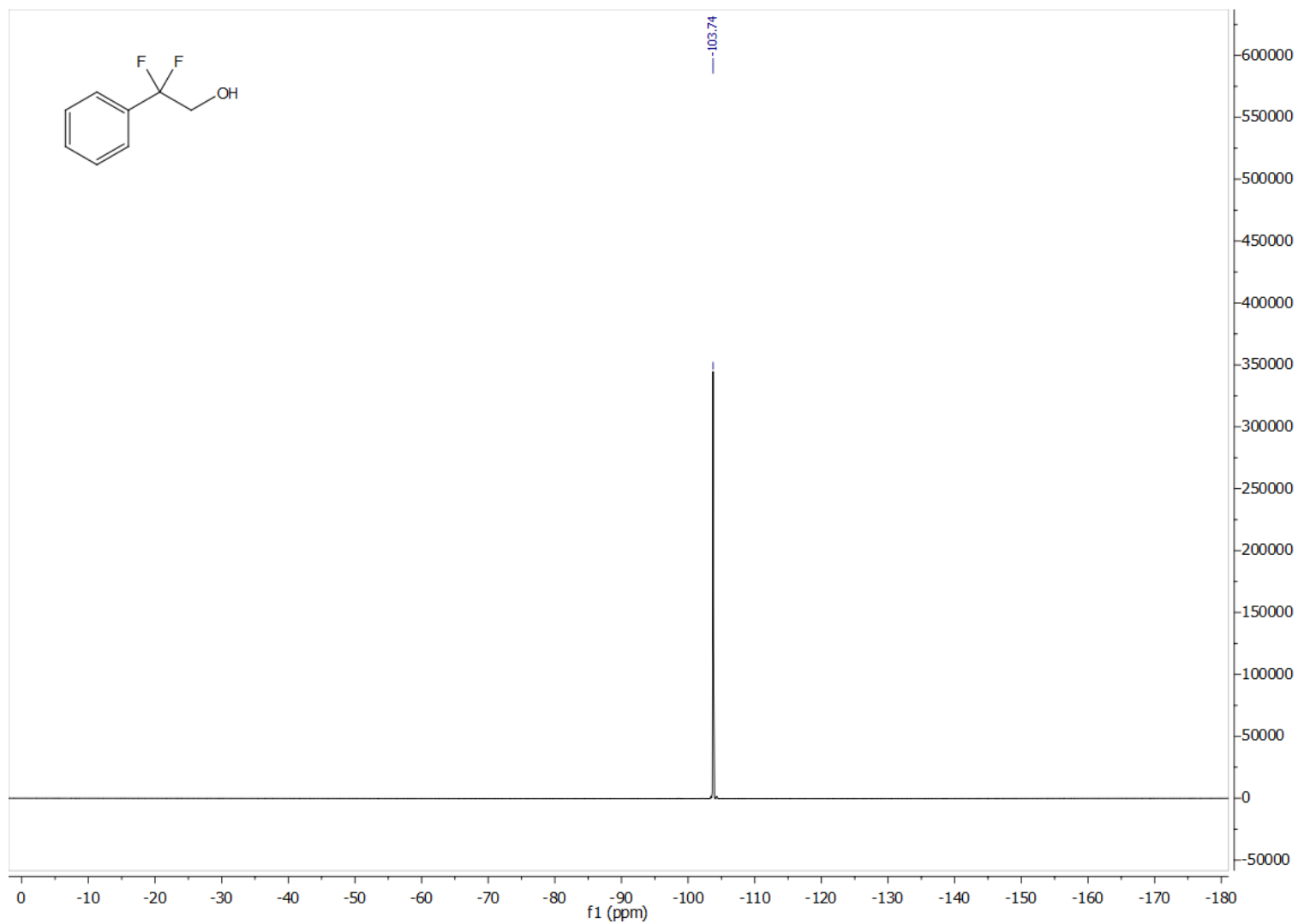


Figure A9: ^{19}F -NMR spectrum of 2,2-difluoro-2-phenylethanol **2**.